Environmental and Experimental Botany 228 (2024) 105986

Contents lists available at ScienceDirect

Environmental and Experimental Botany

journal homepage: www.elsevier.com/locate/envexpbot

Research paper

From landraces to haplotypes, exploiting a genomic and phenomic approach to identify heat tolerant genotypes within durum wheat landraces

Nadia Palermo [a,b], Valentina Buffagni [a], Filippo Vurro [b], Giorgio Impollonia [c], Domenico Pignone [d], Michela Janni [b,*], Henry T. Nguyen [e], Elena Dembech [b], Nelson Marmiroli [a,f]

[a] Department of Chemistry, Life Sciences and Environmental Sustainability, University of Parma, Parco Area delle Scienze, 11/A, Parma 43124, Italy
[b] Institute of Materials for Electronics and Magnetism (IMEM), National Research Council (CNR), Parco Area delle Scienze 37/A, Parma 43124, Italy
[c] Department of Sustainable Crop Production, Università Cattolica del Sacro Cuore, Piacenza 29122, Italy
[d] Institute of Bioscience and Bioresources (IBBR), National Research Council (CNR), Via Amendola 165/A, Bari 70126, Italy
[e] Division of Plant Sciences, University of Missouri, Columbia, MO, USA
[f] CINSA Inter University Consortium for Environmental Sciences, Parma, Venice, Italy

ARTICLE INFO

Keywords:
Durum wheat
Natural germplasm
sHsp26
Heat stress
Phenotyping
SNPs

ABSTRACT

Dry and hot climates severely impact wheat yields, necessitating the development of innovative solutions to accelerate the breeding and selection of more adaptable durum wheat genotypes. The aim of this study was to identify new wheat ecotypes that can bridge the gap between commercial varieties and adaptability to ongoing climate change. In this study, advanced genomic and phenomic techniques were combined to characterize a set of durum wheat landraces derived from single seed descent (SSD). This approach enabled the identification of novel variability in the *TdHsp26-A1* and *-B1* genes. As a result, 38 durum wheat genotypes were analyzed using targeted enrichment PCR, leading to the identification of 17 novel haplotype combinations with SNPs in the TdHsp26 genes. The response of these SSD haplotypes to heat stress was characterized at both the seedling and tillering growth stages. Phenotypic analysis of contrasting genotypes led to the selection of two distinct genotypes: SSD69 and SSD397. During heat stress, SSD69 exhibited altered accumulation of H_2O_2 and MDA content under both growth conditions, providing new insights into the oxidative response to heat stress. Additionally, this work identifies phenotypic traits that are suitable for detecting differences between variants. The geographic distribution of the different alleles aligned with the spread of durum wheat from its center of origin.

1. Introduction

Durum wheat (Triticum turgidum L. subsp. durum (Desf.) Husn. = Triticum durum Desf.) is a crucial cereal crop (Ceglar et al., 2021). The growing global population demands increased food production in the coming years. However, climate change and the diminishing availability of arable land pose significant threats to durum wheat yields, particularly as the crop is primarily cultivated in semi-arid and Mediterranean regions (Ceglar et al., 2021; Fontana et al., 2015; Giovenali et al., 2023; Guzman, 2016; Royo et al., 2014; Xynias et al., 2020; Zampieri et al., 2020). The flowering and grain filling stages are especially sensitive to heat stress (Barlow et al., 2015; Lu et al., 2022; Pradhan et al., 2020), leading to reductions in grain number, yield, and quality (Nuttall et al., 2015; Shirdelmoghanloo et al., 2016; Ullah et al., 2020). To mitigate the effects of climate change and heat stress, new sources of genetic variation are urgently needed (Ullah et al., 2021).

To this end, international collaborative efforts within the Global Durum Wheat Panel (GDP) have produced a collection of 1011 genotypes, capturing 94–97 % of the original diversity representative of modern Triticum turgidum ssp. durum germplasm and landraces, along with selected emmer and primitive tetraploids. These efforts aimed to maximize genetic diversity (Mazzucotelli et al., 2020). The genetic resources available in various germplasm banks offer a valuable reservoir of genetic variability, helping to compensate for the genetic diversity lost due to decades of strong selection focused primarily on yield (Bassi et al., 2016; Borrill et al., 2019).

Previous studies by Marmiroli and colleagues (Janni et al., 2020) highlighted the importance of heat shock proteins (HSPs), particularly

* Corresponding author.
E-mail address: michela.janni@imem.cnr.it (M. Janni).

https://doi.org/10.1016/j.envexpbot.2024.105986
Received 26 April 2024; Received in revised form 16 September 2024; Accepted 23 September 2024
Available online 4 October 2024
0098-8472/© 2024 The Authors. Published by Elsevier B.V. This is an open access article under the CC BY-NC-ND license (http://creativecommons.org/licenses/by-nc-nd/4.0/).

small HSPs 26, in wheat's resistance to heat stress and their relevance for selection (Janni et al., 2020; Maestri et al., 2002). The *TdHsp26* gene family comprises four functional genes, three located on the short arm of chromosome 4 A and one on the short arm of chromosome 4B (Comastri et al., 2018). TdHSP26 is characterized by a central α-crystalline domain (ACD), essential for dimerization and higher-order assembly. The N-terminal domain participates in substrate binding and binds denatured proteins, while the C-terminal domain is involved in homo-oligomerization and the formation of high-temperature stress granules (Basha et al., 2006; Bondino et al., 2012; Comastri et al., 2018).

The *TdHsp26* genes are differentially regulated under direct heat stress and particularly after acclimation. During direct heat stress at 42°C for 2 hours, *TdHsp26-A1* shows significant upregulation, followed by *TdHsp26-B1*, which is more highly expressed when heat stress occurs after acclimation. *TdHsp26-A2*, although exhibiting lower expression levels, is induced 1 hour post-acclimation at 25°C, with its accumulation increasing by 46 % after 24 hours of acclimation following heat stress (Comastri et al., 2018).

Overexpression of *Hsp26* in Arabidopsis promotes germination under heat stress, whereas antisense Arabidopsis plants for *Hsp26* exhibit negligible tolerance even to non-lethal heat shock, with impaired basal thermo-tolerance, reduced biomass accumulation, and lower seed yield under normal growth conditions (Chauhan et al., 2012). Furthermore, in soybean, overexpression of *GmsHsp26* enhances the accumulation of SOD and POD and reduces MDA levels (Liu et al., 2022).

Breeding new varieties is crucial in the era of climate change, as existing genetic resources are increasingly at risk of failing. Various strategies are being explored to identify new traits, including new breeding techniques (Anand et al., 2023; Jenkins et al., 2023), marker-assisted selection (MAS) (Hasan et al., 2021), TILLING (Comastri et al., 2018), and ecotilling (Backes, 2013).

This study originally investigated the genetic variability within a collection of Single Seed Descent (SSD) genotypes (Pignone et al., 2015) using an innovative genomic approach to select genotypes carrying natural mutations in the *TdHsp26-A1* and *-B1* genes. The response to heat stress was evaluated at two developmental stages—seedlings and tillering—to identify ecotypes with contrasting heat stress responses. The relevant phenotypes were identified through a comprehensive analysis of morphological traits, biochemical parameters (such as oxidative stress markers), and gene expression profiles (Akter and Rafiqul Islam, 2017; Chandrasekhar et al., 2017; Hieno et al., 2019; Mohi-Ud-Din et al., 2021; Tardieu and Tuberosa, 2010).

In this work, a core set of durum wheat landraces, selected through Single Seed Descent (SSD genotypes) (Danzi et al., 2022, 2019; Pignone et al., 2015), were tested under heat stress at two developmental stages. A multiple phenotyping approach was used to assess the contribution of the *TdHsp26* genes to the heat stress response. The role of heat shock factors (HSF) and heat shock proteins (HSP), particularly in preventing protein denaturation, sensing reactive oxygen species (ROS), and regulating redox-related genes, was considered. Previous findings on the role of *TdHsp26* in preventing the irreversible aggregation of denaturing proteins (Comastri et al., 2018; Janni et al., 2020; Wang et al., 2014) were also considered.

The discussion focused on the potential of the different single nucleotide polymorphisms (SNPs) identified within these two genes. This study offers new perspectives on the identification and utilization of novel genotypes with targeted gene variations, providing a fresh approach to selecting crop varieties with enhanced resistance to heat stress. Such resilient agrotypes can serve as a valuable genetic foundation for developing crops with greater resilience to climate change (Galluzzi et al., 2020).

2. Material and methods

2.1. Plant materials and experiment layout

Thirty three durum wheat genotypes were analysed as a core set of single seed descent of durum wheat collection (SSD), developed by IBBR-CNR in Bari (Pignone et al., 2015) and selected on phenotypic basis (Danzi et al., 2022, 2019).

The entire SSD collection is represented by 450 genotypes originated in 45 countries around the entire world. The collection has been characterized for its genomic, morphological, phenotypic and quality traits. On this basis, a core set of 152 genotypes (Janni et al., 2018) was finally selected. The core set has been further selected for drought tolerance through high throughput phenotyping based on the water content estimated through Near Infrared (NIR) images (Danzi et al., 2022), leading to a coreset of 33 genotypes.

Here, the SSD used in the allele mining approach and their country of origin are listed in Suppl. Table1. Five commercial varieties (Svevo, Saragolla, Cappelli, Colosseo and Kronos) were also included as references in the allele mining approach for a total of 38 genotypes (33 SSD + 5 varieties). However, due to the limited availability of seeds, the core set was reduced to 30 genotypes (28 SSDs + 2 varieties) in the heat stress test in seedlings, considered representative of the entire genetic variability contained in the SSD core set.

An allele mining approach based on PCR targeted resequencing by NGS technology combined with Kompetitive Allelic specific PCR (KASP) molecular markers, was applied.

Durum wheat germplasm is conserved in the Genebank of the Institute of Bioscience and Bioresources (Mediterranean Germplasm Database -MGD- https://www.ibbr.cnr.it/mgd/) of the Italian National Research Council (CNR-IBBR). Some 80 genotypes of the core set SSD collection joined the Global Durum Panel (GDP).

2.2. DNA extraction and gene targeting

Genomic DNA was extracted with the GenElute™ Plant Genomic DNA Miniprep Kit (Sigma-Aldrich) from leaves tissues of durum wheat genotypes and analyzed through an allele mining approach that combines targeted enrichment PCR with NGS as described in Buffagni et al., 2018.

Within the *TdHsp26* gene family, *TdHsp26-A3* was excluded because it has been classified as pseudogene. Moreover, *TdHsp26-A2* showed week expression under heat stress and for this reason, *TdHsp26-A1* and *-B1* have been considered for this analysis.

The genomic region corresponding to *TdHsp26-A1 (LT220905)* and *TdHsp26-B1 (LT220911)*, 1171 bp and 2575 bp respectively were amplified by PCR to identify SNPs in the SSD genotypes as listed in Table 1 (Comastri et al., 2018).

TdHsp26-A1 and *TdHsp26-B1* (total 3.74 kb Mb) were targeted by PCR with 3 homeologous-specific primer pairs (PPs), 1 for *TdHsp26-A1 (PP1,* Tables 1), and 2 for *TdHsp26-B1* and PP3 for *TdHsp26-B1*. PCR was performed in 25 μL final volume, using TaqDNA Polymerase (New England BioLabs, Hitchin, UK), 10–20 ng template DNA, 0.2 μM of each forward and reverse primers, 0.2 mM of each dNTPs, 1X Standard Taq Buffer (New England BioLabs). All the DNA of the SSD genotypes was provided by IBBR-CNR (Bari, Italy).

PCR amplification with PP2 was performed with touch-down PCR as follows: 1) initial denaturation at 95° for 2 min 2) 10 cycles at 94 °C for 25 s, annealing at 66°C for 30 s with a drop −0.5°C/cycle, elongation at 72 °C for 1 min 30 s, 3) 35 cycles of 94 °C for 25 s, annealing at 61°C for 45 s, elongation at 72 °C for 1 min 30 s, 4) 1 cycle at 72°C for 10 min.

PCR amplifications with PP1 and PP3 were performed with, 1) initial

Table 1
Homoelogous-specif primer pairs (PPs) used in the targeted enriched PCR for *TdHsp26-A and B* genes.

Target	*Homoeologous-specific primer pairs (PPs)*	*Forward 5' – 3'*	*Reverse 5' – 3'*
TdHsp26-A1	*PP1*	*TGTTGGGCCTCCTGATCG*	*AGCCTCAGATGCAGGGTAC*
TdHsp26-B1	*PP2*	*CAATTGGTTCGCACAAACAC*	*CCCTCCAGGCACGGATG*
TdHsp26-B1	*PP3*	*GACACTCTCTCGTTTCAATTCTC*	*GTTATCAGCTTCTTCCGGG*

The target gene on which primers have been designed are indicated. Both forward and reverse primers in 5'-3' are reported.

Table 2
SNPs identified in *the TdHsp26-A1* and *-B1* sequences.

GENE	POOL	SNP ID	REFERENCE POSITION	NUCLEOTIDE IN WILDTYPE	SSD SNP	ALLELE FREQUENCY	POSITION IN THE GENE	TYPE OF MUTATION	EFFECTS
tdHsp26-A1	lib4	SNP a1	2086	G	T	14,83	PROMOTER		
tdHsp26-A1	LIB1	SNP a2	2102	G	C	6,80	PROMOTeR		
tdHsp26-A1	LIB1	SNP a5	2469	G	C	68,52	EXON1	MISSENSE	**Gag/Cag (E73Q**
tdHsp26-A1	LIB2	SNP a5	2469	G	C	29,31	EXON1	MISSENSE	**Gag/Cag (E73Q)**
tdHsp26-A1	LIB3	SNP a5	2469	G	C	46,37	EXON1	MISSENSE	**Gag/Cag (E73Q**
tdHsp26-A1	LIB4	SNP a5	2469	G	C	80,65	EXON1	MISSENSE	**Gag/Cag (E73Q)**
tdHsp26-A1	LIB1	SNP a8	2929	G	A	68,52	EXON2	MISSENSE	**gCc/gAc (G196D)**
tdHsp26-A1	LIB2	SNP a8	2929	G	A	30,02	EXON2	MISSENSE	**gCc/gAc (G196D)**
tdHsp26-A1	LIB3	SNP a8	2929	G	A	46,32	EXON2	MISSENSE	**gCc/gAc (G196D)**
tdHsp26-A1	LIB4	SNP a8	2929	G	A	80,47	EXON2	MISSENSE	**gCc/gAc (G196D)**
tdHsp26-B1	LIB1	SNP b2	597	G	T	7,57	PROMOTeR		
tdHsp26-B1	LIB1	SNP b3	633	A	T	11,54	PROMOTeR		
tdHsp26-B1	LIB3	SNP b4	1212	G	A	21,41	PROMOTeR		
tdHsp26-B1	LIB3	SNP b5	1250	G	A	14,79	PROMOTeR		
tdHsp26-B1	LIB2	SNP b5	1250	G	A	5,48	PROMOTeR		
tdHsp26-B1	LIB3	SNP b6	1287	A	G	96,18	PROMOTeR		
tdHsp26-B1	LIB1	SNP b6	1287	A	G	98,92	PROMOTeR		
tdHsp26-B1	LIB2	SNP b6	1287	A	G	94,14	PROMOTeR		
tdHsp26-B1	LIB4	SNP b6	1287	A	G	99,79	PROMOTeR		
tdHsp26-B1	LIB3	SNP b18	1570	C	G	4,72	PROMOTeR		
tdHsp26-B1	LIB3	SNP b19	1596	G	C	4,63	PROMOTeR		
tdHsp26-B1	LIB3	SNP b25	1647	A	C	5,17	PROMOTOR		
tdHsp26-B1	LIB3	SNP b26	1667	A	G	5,09	5UTR'		
tdHsp26-B1	LIB4	SNP b59	2180	A	G	46,37	EXON2	MISSSENSE	**Atg/Gtg (M97V)**

GENE, indicates in which gene the mutation was found; POOL into which the PCR of the 38 genotypes were grouped, SNP ID, name of SNPs, REFERENCE POSITION, refers to the position upstream the ATG (starting codon), which has been considered as +1, NUCLEOTIDE IN WILD TYPE nucleotide in the TdHsp26-A1 and TdHsp26-B1 sequence in the reference genome, SSD SNP, SNP in the TdHsp26-A1 and TdHsp26-B1 SSD sequence; ALLELE FREQUENCY, mutation frequency in the DNA pools analysed, POSITION ON THE GENE, position of the mutation in the gene, TYPE OF MUTATION, indicates if the mutation is sense, missense, non-sense, EFFECTS, effect on the sequence and on the amino acid composition of the protein.

denaturation at 95°C for 2 min, 2) 35 cycles at 95°C for 30 s, annealing at 60°C for 60 s, elongation at 72 °C for 2 min, 3) 1 cycle at 72°C for 10 min. PCR products were checked on TAE agarose gel to ensure that a specific amplification of the targeted region has occurred.

PCR products were sequenced with BigDye™ Terminator v3.1 Cycle Sequencing Kit (Thermofisher Scientific, Waltham, MA) according to the manufacturer instructions for identity confirmation as described in (Buffagni, 2019), 3 PCR reaction for all 38 genotypes were performed in 96 wells and then pooled in 4 tubes as follows: pool1 (SSD35, SSD92, SSD122, SSD171, SSD253, SSD269, SSD416, SSD487. SSD494 and cv. Kronos), pool2 (SSD44, SSD109, SSD178, SSD322, SSD343, SSD397, SSD415, SSD511, cv. Colosseo), pool 3 (SSD69, SSD99, SSD116,

SSD244, SSD335, SSD409, SSD441, SSD451, cv. Cappelli and cv. Saragolla), pool 4 (SSD64, SSD112, SSD135, SSD195, SSD278, SSD325, SSD459, SSD499, Svevo). Each pool of PCR products was sequenced with the Illumina NovaSeq6000 (Novogene, Beijing, China).

2.3. Bioinformatics analysis of the NGS data

The paired-end (PE) reads raw data from the NGS were checked for QC using FastQC (http://www.bioinformatics.babraham.ac.uk/projects/fastqc/). The two fastq files of the PE of each sample were aligned to Kronos reference genome v.1.1 (https://opendata.earlham.ac.uk/opendata/data/Triticum_turgidum/EI/) using BWA (version 0.7.17) with parameters as default to generate the SAM files. Samtools (version 1.7) was used to convert the SAM to sorted BAM files for each sample. The BAM files were directly visualized with the Integrative Genomic Viewer IGV v. 2.4 (Broad Institute, USA) for the SNP identification and selection. SNPs with a frequency ≥5 % were selected for further investigation.

2.4. KASP assay

Kompetitive Allelic Specific PCR (KASP) was used to identify the SNPs within each pool and to determine the haplotype of each genotype. A primer master mix was made with two allele specific forward primers and one common reverse primer. The primers were designed through software PrimerWeb (http://primer3.ut.ee/) (Untergasser et al., 2012). Oligonucleotides were produced from Sigma-Aldrich (Gillingham, UK) and they present standard FAM or HEX compatible tails (FAM tail: 5′-GAAGGTGACCAAGTTCATGCT-3′; HEX tail: 5′-GAAGGTCGGAGTCAACGGATT-3′). In **Suppl.**Table 2 there is the complete list of primers.

The KASP assay mix was prepared as recommended by LGC Genomics: 46 µl dH_2O, 30 µl of 100 µM common primer and 12 µl of each 100 µM allele-specific primer. The reactions were set up in. 10 µl of final volume, with 10–20 ng of DNA to test.

Wheat Kronos sequence was used as reference, and was considered a wild type control in the KASP analysis. The PCR protocol comprised a 94°C/15 min denaturation, followed by 10 touchdown cycles of 94°C/20 s, 61°C reducing by 0,6°C per cycle/60 s, and 30 cycles of 94∘C/20 s, 55°C/60 s.

2.5. Bioinformatic analysis, in Silico

The promoter analysis was performed with PlantCARE database (Cis-Acting Regulatory Element) (http://bioinformatics.psb.ugent.be/webtools/plantcare/html/) (Lescot, 2002) and PLACE (Plant Cis-acting Regulatory DNA Element) database https://www.dna.affrc.go.jp/PLACE/?action=newplace. (Higo et al., 1999). Through SIFT "Sorting Intolerant From Tolerant" software. The effect that mutations present on exons may have on the functionality of the protein was analyzed (https://sift.bii.a-star.edu.sg/) (Ng and Henikoff, 2003).

2.6. Plant growth and heat stress treatment

Single Seedling Experiment: 40 seeds for each line were sterilized with 10 % (v/v) sodium hypochlorite for 2 minutes in agitation, briefly washed with distilled sterile water, and placed on a filter paper in 9 cm Petri dishes for 7 days at 4°C. The plates, containing 8 seeds for each genotype with a total of 5 plates per line, once germinated, were transferred to the growth chamber with light/dark 18/6 h at 16°C. After 1 week the temperature was raised to 20 °C. Ten-days-old seedlings (two leaves stage, Zadoks Z10) were subjected to heat stress at 38°C for 4 h (4hPS) and recovered for 1 h at 23°C (1hPR). Control plants were kept at 23°C during the experiment. One-week post stress (1WPS), control (C1W), and stressed plants (S1W) were also sampled (**Graphical Abstract**).

Tillering experiment: Based on the results of the seedling experiment, SSD69, SSD178, SSD244, SSD397, SSD415 Svevo and Kronos, were sterilized and placed on wet Whatman filter paper in Petri dishes for 7 days at 4°C. Once germinated, the seedlings were transferred to pots containing 700 g of soil mixture composed by 1:3 peat: perlite sterilized and mixed commercial soil. A total of 16 plants for each SSD were placed in 1,5 L pots, 4 plants each pot. Plants were grown in controlled conditions in a growth chamber, photoperiod light/dark 18/6 h with 18/15°C temperature. At the tillering stage (Zadoks Z31) heat stress was imposed. The day before the stress, the temperature in the chamber was set to 23°C. Temperature was then set to 38 °C for 4 h (4hPS) and recovered for 1 h at 23°C (1hPR). Control plants were kept at 23°C during the entire length of the experiment (**Graphical abstract**). Leaves of control and stressed plants were sampled at the following timepoints:

i) before the heat stress (T0), ii) 4 hours post-stress (4hPS) and iii) 1-hour post-recovery (1hPR). One-week post stress (1WPS) leaves were sampled in both control and stressed plants (C1W and S1W).

2.7. Phenotypic plant traits analyzed

The morphological, physiological and biochemical traits were analyzed and a schematism is reported in the Graphical Abstract.

Traits have been recorded in two phenological stages: seedlings and tillering.

2.8. Morphometric characterization

2.8.1. Seedling stage

C1W and S1W seedlings length were acquired and analysed using ImageJ Software (available at http://rsb.info.nih.gov/ij/ accessed on 20 September 2021; developed by Wayne Rasband, National Institutes of Health, Bethesda, MD, USA). Three biological replicates for each condition were considered.

2.8.2. Tillering stage

Plant height, number of culms, and number of leaves were recorded. Leaf area and canopy of 3 plants for both control and stress plants were recorded at T0, 48hPS (48 hours post stress) and 1WPS. The leaf area was calculated manually using the following formula Leaf area = Length x width x 0.75 (Kuzmanović et al. 2014; Ahmad et al., 2015); while canopy (%) was measured using the CANOPEO cellphone app (Patrignani and Ochsner, 2015).

2.9. Physiological characterization

2.9.1. Stomatal resistance

Stomatal resistance (r_s) was measured using AP4 porometer (Delta-T Devices, UK), that measures stomatal resistance of leaves in $sec.cm^{-1}$. Stomatal resistance was acquired at the following time points: T0, 4hPS, 48hPS and finally after one week post stress in C1W and S1W. Three flag leaves from three plants per plot were measured for stomatal resistance, six readings per genotype.

2.9.2. Infrared Leaf Temperature and Canopy depression temperature (CTD)

Thermal imaging was applied using an infrared thermal camera FLIR E75 to detect variations in the canopy temperature during the stress. The portable thermal camera (FLIR, E75) had a 17 mm lens, a resolution of 320 × 240 pixels, frequency of 30 Hz, spectral range of 7.5–14 µm and a temperature range from −20 to 120 °C, thermal sensitivity lower than 0.03°C.

Emissivity used was 0.99. Measurements were taken at the following time points T0, 4hPS and in C1W and S1W. Three pictures of each plant were acquired. The thermal images were analyzed using R software (R Core Team, 2022) and the Thermimage package (https://cran.r-project.org/web/packages/Thermimage/index.html).

To separate vegetation from the background, only vegetation pixels

were classified by applying k-means clustering algorithm on thermal images. The average canopy temperature for each plant was extracted from pure vegetation pixels.

The canopy temperature depression (CTD) was calculated and defined as the deviation of plant canopy temperature from ambient temperature and was recognized as the key trait to evaluate/compare for the response of each genotype to low water availability, high temperature and other environmental stress.

2.9.3. Relative water content (RWC)

The Relative Water Content (RWC) was measured in leaves following the protocol reported in Celik, (Çelik, et al., 2017). Three leaves were randomly collected to determine relative water contents within each group. After measuring the fresh weights (FW), leaves were placed into distilled water for 12 h in order to obtain turgid weight (TW). Following the TW measurement, leaves were heated in a dry heat incubator for 24 h (80°C) to obtain dry weights (DW). RWC was calculated according to the formula reported by Smart (Smart and Bingham, 1974):

$$RWC = \frac{(FW - DW)}{(TW - DW)} * 100$$

Samples were taken at time T0, 4hPS, C1W and S1W.

2.10. Biochemical analysis

Content of MDA in seedling and tillering stages and H_2O_2 in tillering was measured in leaves at T0, 4hPS, 1hPR, C1W and S1W. Four seedlings for each genotype were sampled, pooled and immediately frozen with liquid nitrogen for biochemical analysis.

2.10.1. Determination of H_2O_2 content

The Hydrogen peroxide (H_2O_2) concentration was determined in tillering stage following (Velikova al., 2008), with some modifications. Leaf tissues (50 mg) were manually homogenized in ice bath with 1 mL 0.1 % (w/v) trichloroacetic acid (TCA) The homogenate was centrifuged at 12,000 g for 15 min at 4°C. Then 250 μL of the supernatant were added to 250 μL 10 mM potassium phosphate buffer (pH 7.0) and 500 μL 1 M KI and the supernatant held 20 min at room temperature, after which the absorbance was read at 390 nm using a Varian Cary 50 spectrophotometer·H_2O_2 content was determined using the extinction coefficient 0.28 μM^{-1} cm^{-1} (Dong et al., 2014); H_2O_2 was expressed as nmol mg^{-1} FW. (Figs. 1–9)

2.10.2. Estimation of malondialdehyde (MDA) content

The effect of heat stress on membrane lipid peroxidation was verified by quantifying the MDA content in seedlings (Z10) and tillering (Z31) stage. In seedlings one genotype for each haplotype combination was randomly selected and analyzed for all five treatments (T0, 4hPS, 1hPR, C1W and S1W). To determine the concentration of MDA the Thiobarbituric Acid (TBA) test was used following the protocol reported in Senthilkumar et al. (2021). 50 mg of leaves grounded in liquid nitrogen, 1 mL were added 0.1 % (w/v) trichloroacetic acid (TCA) to precipitate the proteins. The homogenized samples were then centrifuged at 12, 000 rpm for 15 min. Subsequently, 250 μL of the supernatant was added to 1 mL of 20 % TCA containing 0.67 % TBA. The mixture was boiled at 95°C for 30 min in a water bath and quickly cooled in ice bath for 10 min to stop the reaction. The mixture was centrifuged at 10,000 rpm for 5 min and the supernatant collected. The absorbance was read at 532 and 600 nm to calculate the MDA-TBA concentration based on the Ɛ value with a Varian Cary 50 spectrophotometer. Where, Ɛ is the molecule absorbance (1.55 mM −1 cm −1). The amount of MDA is expressed as nmol mg^{-1}FW in Suppl. Fig. 5 and was calculated according to the formula of Wu et al.,2012.

The relative MDA content variation expressed in percentage (Table 3) was calculated as follow

$$\frac{(MDAcontrol - MDAstressed)}{MDAcontrol} \times 100$$

The MDA ratio was calculated as (MDA stressed 1WPS/ MDA control plants) and was used to develop the radar plot (Fig. 3)

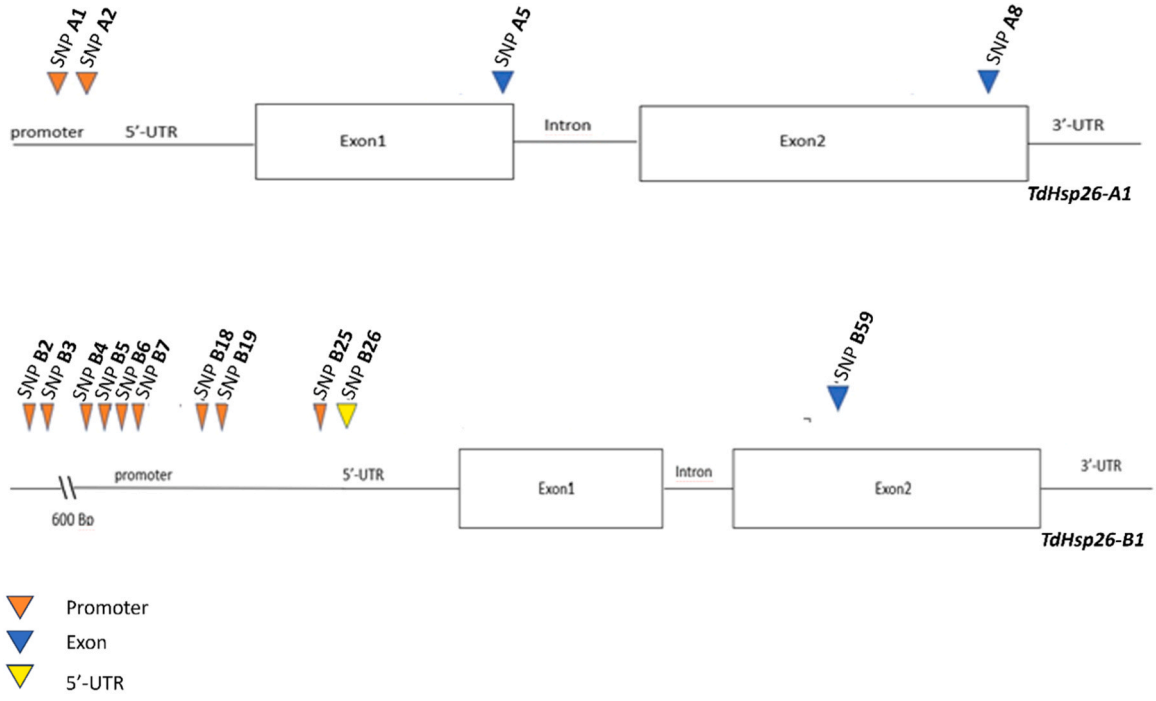

Fig. 1. SNPs position on a) TdHsp26-A1 and b) TdHsp26-B1 gene sequence scheme as previously reported in Comastri et al., 2018). Promoter, 5' UTR, exons, introns and 3'UTR of each gene is reported. Yellow triangles indicate that the SNP is located on 5'-UTR, blue triangles indicate that the SNP is located on Exon2, Orange triangles indicate that the SNP is located on Promoter.

Fig. 2. Geographic distribution of the SSDs under consideration. HA 1:17, number of the haplotype combination (Suppl. Table 5).

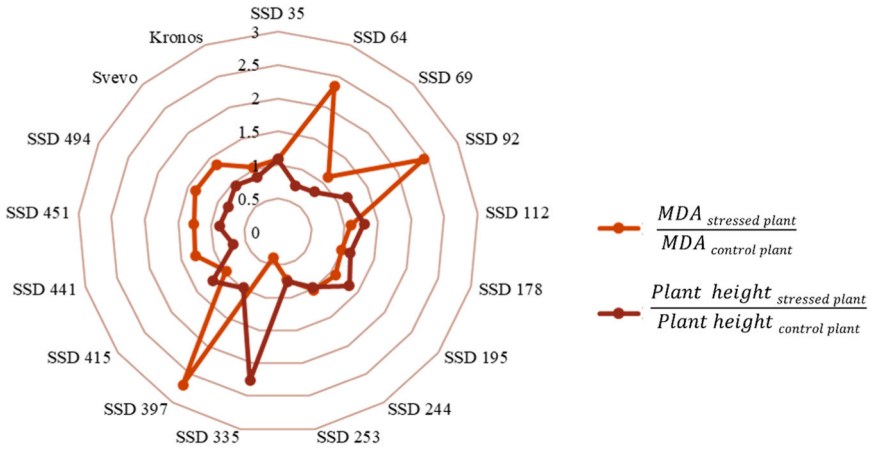

Fig. 3. Radar Plot of MDA ratio content variation and plant height traits. SSD, Single Seed Descent genotypes, MDA, Malondialdehyde. Orange lines, MDA ratio content calculated as MDA stress/MDA control; dark red lines, plant height ratio calculated as plant height stress/ plant height control. One single SSD line representing each haplotype combination has been analysed.

2.11. Stress indices calculated through iPASTIC

To calculate stress tolerance and susceptibility indices for various crop traits, the iPASTIC (*The Plant Abiotic Stress Index Calculator)* software https://manzik.com/ipastic/ (Pour-Aboughadareh et al., 2019) was used. The indices acquired through iPASTIC were tolerance index (TOL), relative stress index (RSI), mean productivity (MP), harmonic means (HM), yield stability index (YSI), geometric mean productivity (GMP), stress susceptibility index (SSI), stress tolerance index (STI) and yield index (YI). The program estimates an Average Sum Ranks (ASR) for all indices to select potentially superior genotypes; the lower was the ASR the more tolerant is the genotype. The grain yield per plant, expressed as the number of seeds per plant, was used to run iPASTIC, to obtain the yield of stressed and not stressed plants for each genotype.

2.12. Reverse transcription Quantitative Real time PCR (RT-qPCR)

In both Z10 and Z31 stages the RNA was extracted using the Rneasy Plant Mini Kit (Qiagen, Hilden Germany). cDNA was generated with QuantiTect Rev.Transcription Kit (Qiagen). Real Time (RT) qPCR analysis was performed using CFX96 Touch Real-Time PCR Detection System (Biorad). PCR reactions were set up in 10 µL containing 1 µL of 1:10 dilution of cDNA, 0,25 nM of gene-copy specific forward and reverse primers A1-PT31F (5'-CCAGGCCCAGAACGCT-3')/A1-PT31R (5'-CCTCCTTcTCGTCCTCCATa-3'), B1-PT10F (5'-CGATGCGGCAGATG CTT-3')/B1-PT10R (5'-TGACGAGCGCGTCGC-3') (Comastri et al., 2018). *TdACT* gene (AB181991) was used as house-keeping.

In seedlings the ΔCt as $Ct_{target\ gene}$—$\Delta Ct_{internal\ standard}$ was calculated and the expression level variations were then expressed as $\Delta\Delta CT = Ct_{treatment} - Ct_{control}$.

In tillering a semiquantitative RT-PCR was applied for *TdHsp26* gene expression. The amplicons were loaded on a 1.2 % agarose gel. The bands were analyzed by imageJ software (https://imagej.net/ij/) and normalized for the band of the housekeeping genes.

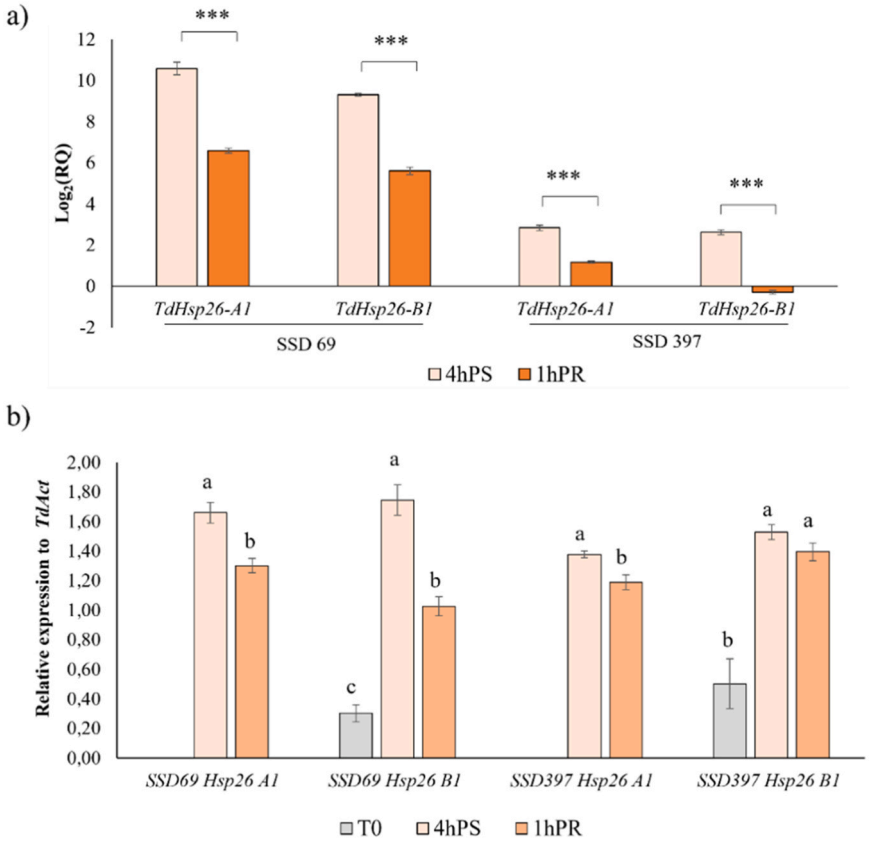

Fig. 4. a) Expression analysis of TdHsp26-A1 and TdHsp26-B1 in SSD69 and SSD397 genotypes at seedlings stage. The induction level is expressed as fold change (rQ) of the treated sample in respect to the control and reported as log2(rQ) in the diagram vertical. Vertical bars indicate the standard error. Student's t-test was applied between 4hPS and 1hPR of each group. **P <0.01, ***P <0.001. b) RT-qtPCR of TdHsp26 at tillering stage. Gene expression was normalized based on the expression values of the reference gene TdAct (ID AB181991). Values shown are mean ± standard error. Different alphabetic letters indicate the significant differences with the ANOVA test (p-value< 0.05). T0, control before the onset of stress under normal growth conditions; 4hPS, 4 hours post stress, 1hPR, 1 hour post recovery.

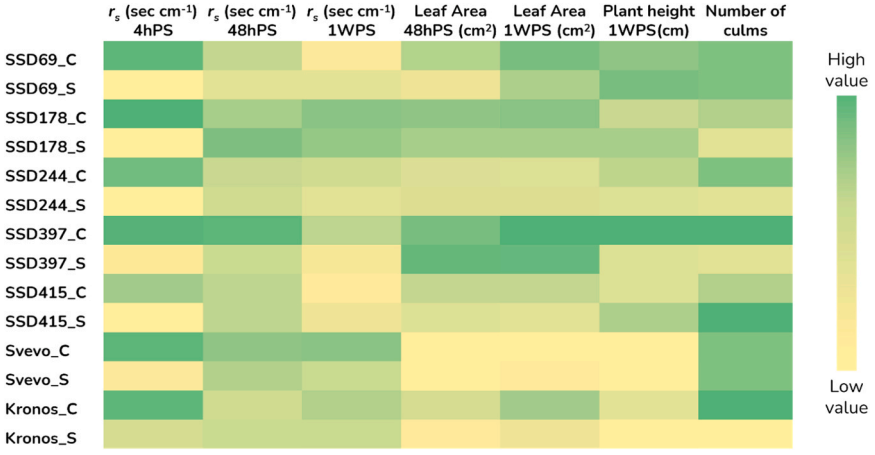

Fig. 5. Heat map of phenotypic traits stomatal resistance, leaf area, plant height, and culm numbers in tillering stage, for control (C) and stressed (S) plants. r_s stomatal resistance; Leaf area, Plant Height, number of culms measured at 4 hours post stress (4hPS), 48 hours Post Stress (48hPS), and 1 week post stress (1WPS). r_s, stomatal resistance expressed in (sec cm^{-1}).

2.13. Protein structure analysis

Sequences of TdHSP26-A1Kr (AF-A5A8V2-F1-model_v4) and TdHSP26-B1Kr (AF-A5A8V1-F1-model_v4) protein were downloaded for structural and functional analysis from AlphaFold (10.1038/s41586–021–03819–2). Both models were graphically visualized with Pymol 3.0 (The PyMOL Molecular Graphics System, Version 2.0 Schrödinger, LLC.).

Multiple alignment of amino acid sequences was performed using Clustal Omega (10.1002/0471250953.bi0313s48.) and displayed with graphical enhancements using ESPript 3.0 (10.1093/nar/gku316).

Protein sequences were searched with PSort I (plant sequences)

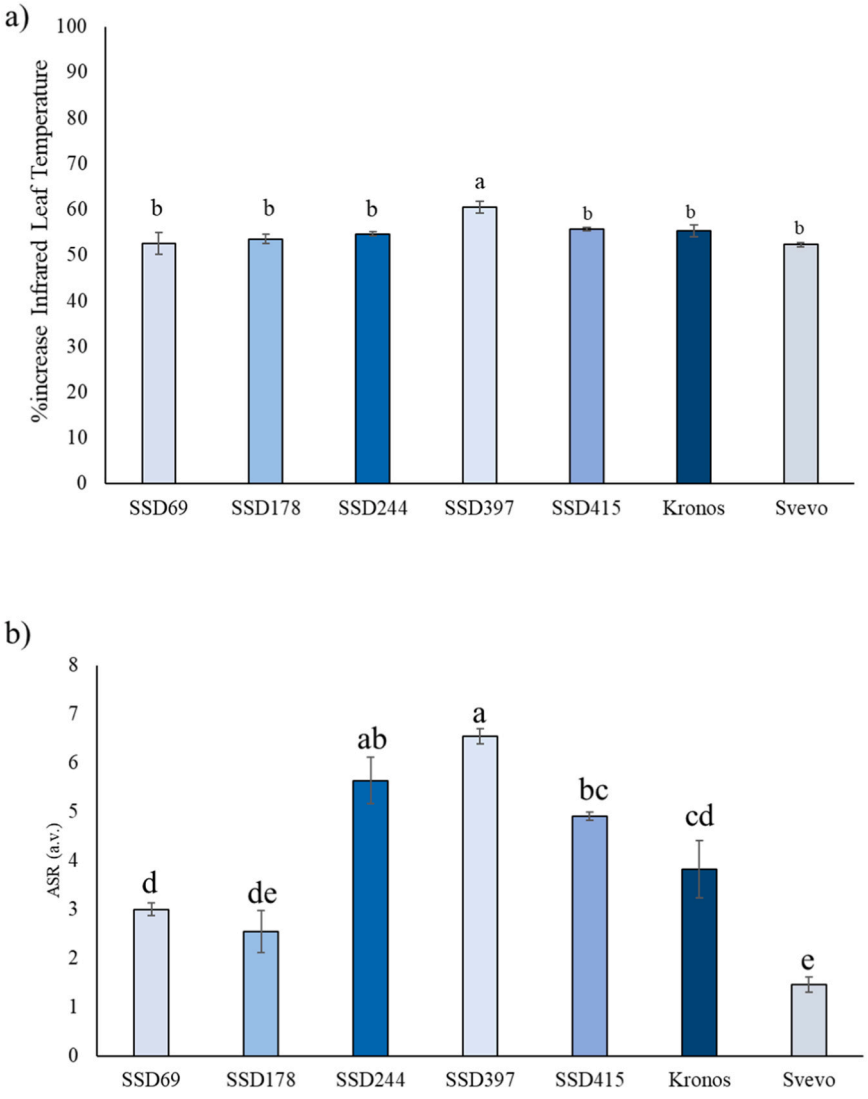

Fig. 6. a) Percentage of increased Infrared Leaf Temperature measured with thermal camera at time T0 and after 4 hours post stress (4hPS) at 38°C for each genotype. b) Average Sum Ranks (ASR) of the analyzed SSDs at Zadoks 31. a.v = absolute value. Average Sum Ranks (ASR), that includes: Tolerance, Mean Productivity, Geometric Mean Productivity, Harmonic Mean, Stress Susceptibility Index, Stress Tolerance Index, Yield index, Yield Stability Index and Relative Stress Index. The different alphabetical letters in superscript indicate the significant differences at $P < 0.05$ according to the ANOVA test. Error bars represent the standard errors.

server (10.1016/s0968–0004(98)01336-x) to make predictions about protein cellular localization.

2.14. Statistical analysis

For the experiments with seedlings: Student t-Test was applied to analyze the difference in plant height and for the analysis of gene expression data. For data analysis on MDA content, ANOVA test with p-value <0.05 was performed using Past 4.03 software, the next post hoc used was Tukey's test. In the tillering experiment: leaf area, number of culms, plant height, stomatal resistance, CTD, and gene expression were analyzed by Student *t*-Test. Infrared leaf temperature, average sum of ranks, H_2O_2 and MDA were analyzed by ANOVA test with p-value <0.05 using Past 4.03 software, the next post hoc used was Tukey's test. Principal component analysis (PCA) was performed using the R statistical software version 4.2.1.

3. Results

3.1. Germplasm genetic variability in TdsHsp26-A1 and TdsHsp26-B1, SNPs identification

To identify natural allelic variants in the *TdHsp26* genes, a targeted resequencing strategy was employed to perform allele mining in a set of durum wheat landraces and five reference varieties selected for their performance under heat stress (Buffagni, 2019). Targeted resequencing is a PCR-based approach that enables the sequencing of specific genes of interest using next-generation sequencing (NGS) prior to identifying full-length target sequences. In this study, multiple overlapping PCR products were generated, covering the entire targeted sequences of both *TdHsp26-A1* and *TdHsp26-B1* genes. This approach also involved pooling the DNA of targeted genotypes to increase throughput and applying KASP markers for SNP detection to facilitate SNP identification and reduce costs.

Based on this strategy, a list of SNPs was identified, with only those

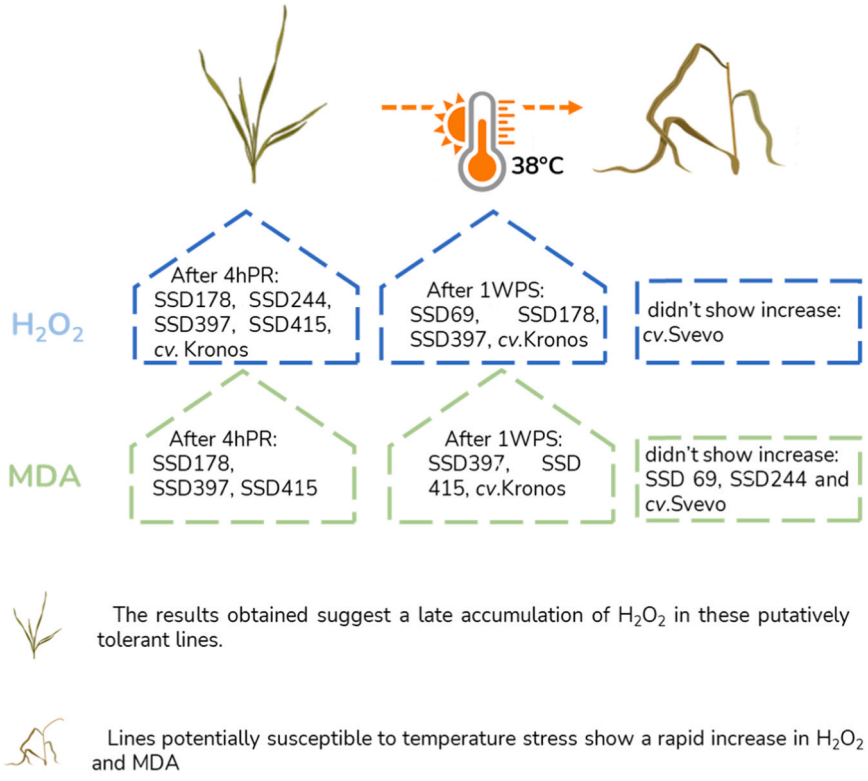

Fig. 7. Outline of the results obtained from the analysis of H_2O_2 and MDA.

having a frequency greater than 5 % being selected, given that 99 % homozygosity was expected in all loci for the 33 SSD genotypes and the five selected cultivars.

A total of 72 polymorphic sites were identified (8 for *TdHsp26-A1* and 64 for *TdHsp26-B1*) with frequencies ranging from 4.63 % to 99.79 %. Each pool was generated by amplifying target sequences from 9 (pool 2, pool 4) or 10 genotypes (pool 1, pool 3), so it was expected that a single variant would be represented with a frequency of about 10 %. Under conditions of 99 % homozygosity at all loci, a 9–10 % SNP frequency was expected for a single genotype variant. Therefore, all variants with a frequency below 5 % were considered false positives, while SNPs with a frequency of 5 % or higher were selected for further investigation using KASP technology.

Fifteen SNPs were identified: three were located in the coding sequence (CDS), two in the promoter region of the *TdHsp26-A1* gene, nine in the promoter region of the *TdHsp26-B1* gene, and one in the 5'-UTR of the *TdHsp26-B1* gene. Missense mutations were also found, including one in *TdHSP26-B1* (amino acid variant M97V) and two in TdHSP26-A1 (amino acid variants E73Q and G196D). The higher rate of variability in regulatory elements may enhance the gene's role in adapting to challenging agro-climatic conditions.

The KASP assay confirmed the detected SNPs and allowed for the assignment of mutations to specific genotypes (Table 2). The SNP frequency for a single genotype ranged from 5 % to 16 %, likely due to an imperfect relative balance of PCR products during the pooling of samples.

3.2. Haplotype selection and heat stress experiment

Based on the SNPs identified, a total of fourteen haplotypes, five for *TdHsp26-A1* and nine for *TdHsp26-B1* genes, were identified. The SNP B6 is located in *TdHsp26-B1* promoter and is present in all genotypes except for SSD322 and SSD415. SSD195 showed 3 SNPs in *TdHsp26-A1*. The SSD244 showed the greater number of mutations on promoter of *TdHsp26-B1*. A total of 17 haplotype combinations (HA) were identified in both *TdHsp26-A1 and TdHsp26-B1* (Fig. 1**, Supp. Table 5.**).

A haplotype combination (HA) is defined as a genotype carrying multiple identified SNPs (Fig. 2). The effects of mutations in the regulatory elements (cis-acting elements) of the TdHsp26 promoter sequence were assessed using PLACE and PlantCARE databases. Several SNPs—B2, B4, B6, and B25—were identified in the promoter of the *TdHsp26-B1* gene. SNPs B4 and B6 result in the loss of two cis-acting elements associated with plant responses to environmental factors: GT1CONSENSUS, involved in light and salicylic acid response (Villain et al., 1996), and GTGANTG10, which plays a role in primary metabolism and the regulation of pollen-specific gene expression (Rogers et al., 2001). Conversely, SNPs B2 and B25 lead to the formation of two new cis-acting elements: RYREPEATBNNAPA, involved in seed-specific expression (Ezcurra et al., 2000), and DPBFCOREDCDC3, associated with bZIP class transcription factors in carrots (Ramkumar et al., 2015) (Supp. Table 3). The SNPs identified in the promoter region of TdHsp26-A1 did not result in significant changes in this regulatory region.

To predict the impact of amino acid substitutions on protein function, in-silico analysis was conducted using SIFT software, which evaluates the potential effects of mutations based on sequence homology and the physical properties of amino acids (Ng and Henikoff, 2003). The software returns a score ranging from 0 to 1, with scores >0.05 indicating tolerated SNPs and scores <0.05 suggesting potentially deleterious effects. None of the SNPs identified in this study were predicted to be deleterious.

SNP A5 (found in HA4, HA5, HA6, HA7, HA8, HA10, HA11, HA15), SNP A8 (found in HA3, HA4, HA5, HA6, HA8, HA11), and SNP B59 (found in HA6) were analyzed using SIFT. These SNPs are located in Exon 1 and 2 of the *TdHsp26-A1* gene and Exon 2 of the *TdHsp26-B1* gene, respectively, and all are involved in missense mutations (Supp. Table 4). SNP A8, which causes a G196D substitution in the α-crystallin domain—a region characterized by two highly conserved areas (Bondino et al., 2012)—is of particular interest, as the presence of a SNP in this region may suggest a potential deleterious effect on protein

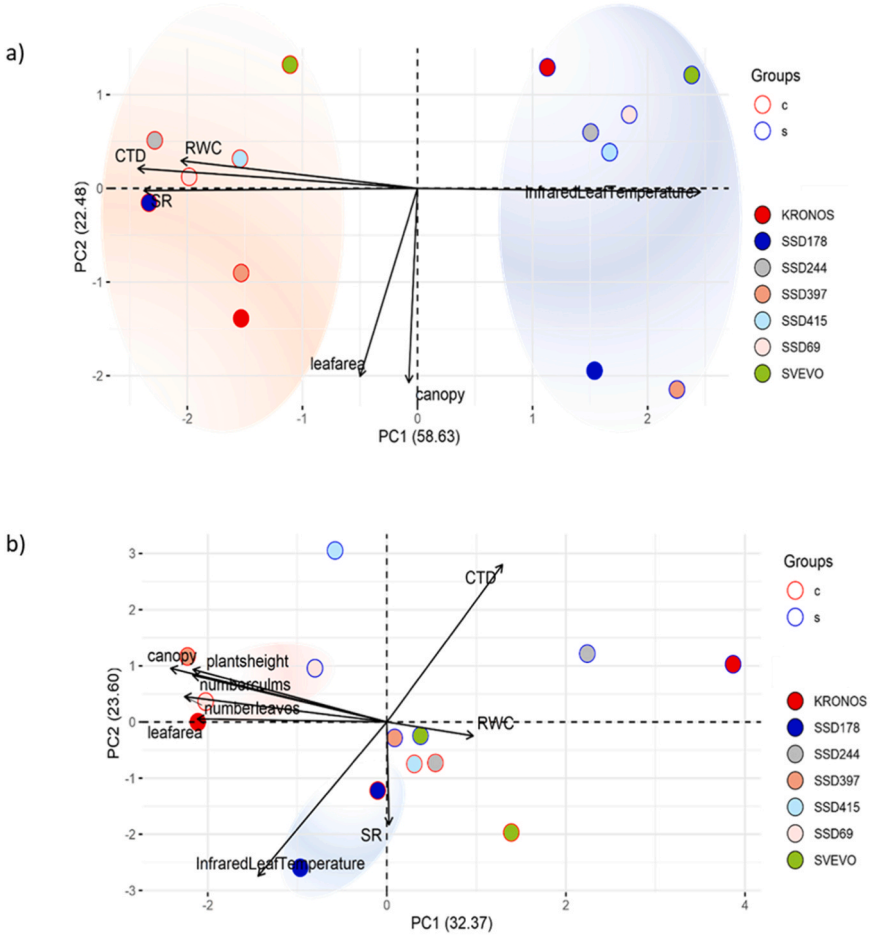

Fig. 8. Principal component analysis (PCA) of the effect of heat stress imposed in the tillering stage in 7 SSD genotypes previously selected. a) Biplot at 4 hours post stress (4hPS), the two colors define the two different clusters, blue includes all controls, red all stressed b) Biplot 1 week post stress (1WPS) the pink and blue shade indicates the potentially tolerant genotypes 69 and 178 respectively. RWC, Relative Water Content; CTD, Canopy Temperature Depression; leaf area, canopy, SR, Stomatal Resistance, Infrared leaf temperature; Plants height, Numbers of culms, Numbers of leaves.

function.

SNP B59 results in the smallest reduction in protein tolerance to the change (SIFT value 0.10), followed by SNP A5 (SIFT value 0.23). Despite being located in the α-crystallin domain, SNP A8 is considered tolerable (SIFT value 1).

Further analysis of the protein sequence and structure for TdHSP26-A1Kr variants (SNP A5 and SNP A8) and the TdHsp26-B1Kr variant (SNP B59) (Suppl. Fig. 6, Suppl. Fig. 7) revealed that SNP A5, where glutamate 73 is replaced by glutamine (E73Q, Suppl. Fig. 6), leads to the acquisition of an amino group that replaces a negatively charged carboxyl group. However, this residue is located in a region of the protein predicted to lack secondary and tertiary structure (Suppl. Fig. 7a), making it difficult to determine its role and whether the loss of the carboxylic group prevents crucial interactions or coordination. SNP A8 causes the replacement of glycine with aspartate at position 196, resulting in the acquisition of a negatively charged carboxyl group (G196D, Suppl. Fig. 6). This substitution occurs in the middle of the β5-strand (194−200), which forms part of the alpha-crystallin domain, opposite the alpha-helices and close to the hydroxyl group of serine 196 (Suppl. Fig. 7a). Similarly, SNP B59 causes the replacement of methionine with valine at position 97 (M97V, Suppl. Fig. 6), leading to the loss of the S-methyl thioether side chain and altering the steric hindrance at the beginning of the alpha-helix (Suppl. Fig. 7b). These missense mutations could play critical roles in maintaining the chaperone function of the protein and stabilizing overall protein folding.

Computational predictions suggest that both TdHSP26-A1Kr and TdHSP26-B1Kr proteins are likely localized in the thylakoid (Prob = 98.29 %), supported by the presence of the thylakoid lumenal transfer peptide "VASAA" at positions 44–48 (Suppl. Fig. 6, blue columns), aligning with previously predicted subcellular localization (Comastri et al., 2018).

Geographically, the most prevalent haplotypes were HA1, HA2, and HA3. HA2 was primarily found in SSD genotypes originating from North Africa and Mediterranean countries, including Greece, Italy, Algeria, and Ethiopia (Fig. 2). A set of five unique haplotypes (HA10, HA13, HA14, HA15, HA17), each corresponding to a specific SSD genotype, were associated with regions in the Hellenic Peninsula.

The distribution of SNPs is as follows: 46.67 % in Africa, 40 % in the Fertile Crescent, 53.3 % in Europe, and 26.67 % in the Americas. Most of these genetic variations developed within or near the primary (Fertile Crescent) and secondary centers of origin for this species (Ethiopia), with a few exceptions likely emerging later during the global spread of durum wheat cultivation (Supp. Table 5, Fig. 2).

3.3. Natural mutations in the TdHsp26 genes affect the heat stress resistance. Early stress response in seedlings

To investigate the effects of the identified mutation, detailed phenotyping was conducted, focusing on morpho-physiological, biochemical, and yield-related traits under heat stress at two growth stages: seedling and tillering (see Graphical Abstract).

Plant height exhibited three distinct trends: i) SSD44, SSD64, SSD69,

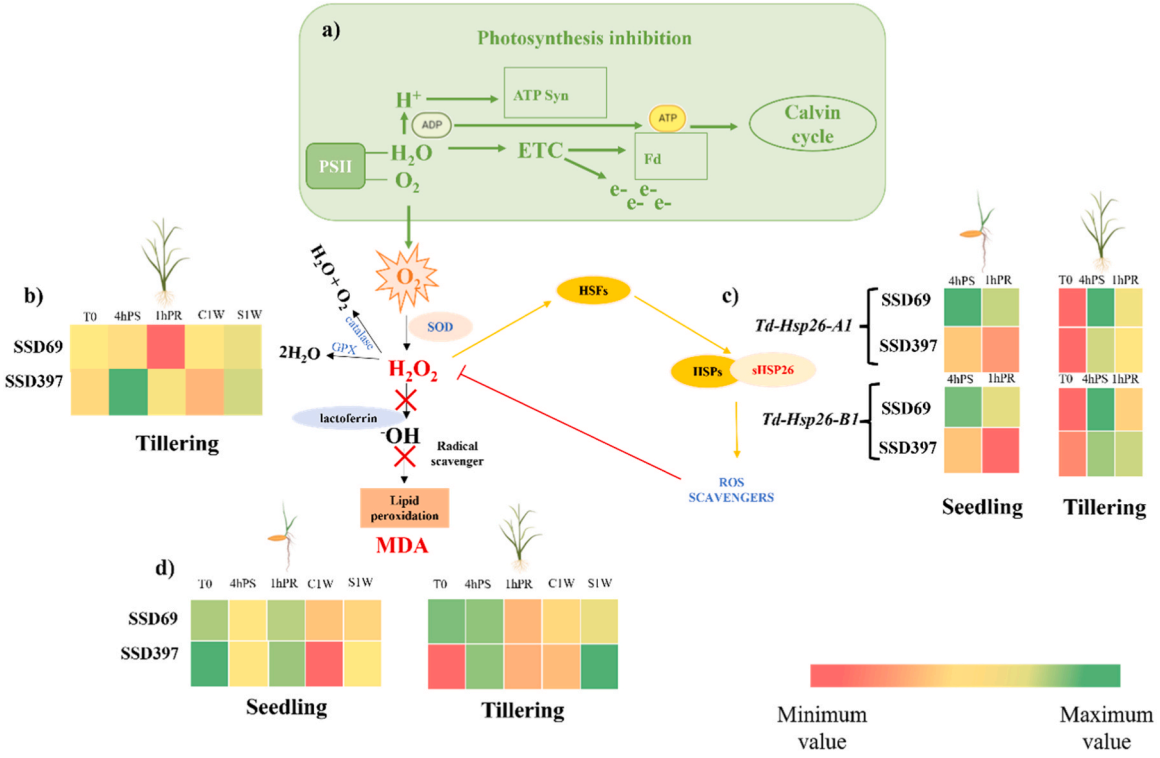

Fig. 9. Possible explanation of the role of TdHSP26 in the ROS cascade. **a)** Calvin cycle photoinhibition scheme. **b)** heat map of H_2O_2 content in tillering stage. **c)** heat map of TdHsp26-A1 and B1 gene expression in seedling and tillering stages. **d)** heat map of MDA content in seedling and tillering stage. Abbreviations: H^+, hydrogen molecule, ADP, adenosine diphosphate; ATP, adenosine triphosphate; H_2O, water; ETC, electron transport chain; e^-, electron; Fd, ferredoxin; PSII, photosystem II; O_2, oxygen molecule; SOD, superoxide dismutase; CAT, catalase; GPX, glutathione peroxidase;H_2O_2, hydrogen peroxide; (•OH), hydroxyl radical, HSFs heat shock transcription factor, HSP, Heat Shock Proteins, sHSP26, small Heat Shock Protein 26. In colored box, graduation of red, decrease in H_2O_2 content MDA content and gene activity; graduation of green, increase in H_2O_2 content MDA content and gene activity.

Table 3
Relative MDA content variation (%) in seedlings over the time of the experiments.

RELATIVE MDA CONTENT VARIATION (%)			
SSD	(T0-4hPS)/T0	(T0-1hPR)/T0	(C1W-S1W)/C1W
35	−19.86	−75.02	9
64	−23.22	−14.54	133.4
69	−18.43	-2.30	11.59
92	1.02	49.28	144.03
112	−15.47	10.66	9.15
178	−26.80	7.47	−0.31
195	−44.73	−31.14	7.93
244	−82.33	−50.53	2.67
253	−5.22	78.36	−27.38
335	0.23	23.78	−60.53
397	−28.85	−10.43	169.75
415	−76.86	−60.27	1.56
441	−35.31	−59.95.	28.28
451	−5.59	−15.88	26.26
494	−1.12	22.85	38.02
Svevo	−38.52	−6.95	36.72
Kronos	−25.24 %	−34.47	25.30

Legend. The relative value of the MDA content was calculated from the following formula: ((MDAcontrol-MDAstressed))/MDAcontrol×100). In the case of 4hPS and 1hPR the reference control is T0, while for S1W the reference is C1W.

SSD109, SSD116, SSD171, SSD253, SSD278, SSD441, SSD451, SSD487, SSD511, and Kronos showed a shorter height compared to the control, indicating a stronger impact of heat stress on this trait; ii) SSD35, SSD92, SSD99, SSD112, SSD122, SSD244, SSD269, SSD397, SSD409, SSD459, SSD494, and Svevo showed no difference between stressed and control conditions; iii) SSD178, SSD195, SSD322, SSD335, and SSD415 were taller than the controls under stress conditions (Suppl. Fig. 1).

Malondialdehyde (MDA) content, a key indicator of oxidative and heat stress, was measured in one SSD genotype representing each haplotype combination. Since MDA is a major breakdown product of polyunsaturated fatty acids in cell membranes, it serves as an important marker of stress. Seedlings of all genotypes were analyzed for MDA content (Suppl. Fig. 2). The SSD lines displayed an unusual pattern, with an increase in MDA during and after heat stress. In wheat plants, MDA content in the first leaf typically decreases immediately after heat treatment and then increases after one hour of recovery (Savicka and Skute, 2010). In SSD35 and SSD441, a gradual reduction of MDA from T0 to 1hPR was observed, whereas the other genotypes showed a sharp decrease after 4 hours of heat stress followed by a significant increase just one hour into recovery. A substantial rise in MDA content was noted at 1WPS in SSD64 and SSD397, with increases of 133.4 % and 169.75 %, respectively; SSD69 showed only a modest increase of 11.59 % at S1W.

To better assess the variation over time, the relative MDA content was calculated (Table 3).

SSD92, SSD253, SSD335, and SSD494 exhibited significant variations in relative MDA content, with a consistent accumulation at 1hPR (Table 3). SSD35 showed marked fluctuations in relative MDA content during the phases of heat stress and recovery.

Interestingly, SSD69 and Svevo displayed no significant changes in relative MDA content immediately after stress (4hPS) and following recovery (1hPR), suggesting a potential correlation with heat stress tolerance (Table 3).

To assess the treatment's effect on each haplotype combination, a radar plot was constructed (Fig. 3), comparing the stress-to-control ratio for plant height and MDA content one week after stress. One genotype from each haplotype combination (HA) was included. Notably, genotypes SSD64, SSD92, and SSD397 showed a greater increase in MDA content between control and stressed plants.

3.4. TdHsp26 gene expression analysis

Based on the results for plant height, MDA content, and SNP positions within the gene, SSD397 and SSD69 were selected for further analysis of gene expression (Fig. 4a).

SSD69 and SSD397 each exhibited unique haplotypes with distinctive SNPs: SSD69 had three SNPs in the promoter region of the *TdHsp26-B1* gene (B4, B6, and B19) and two mutations in the exons of the TdHsp26-A1 gene (A5 and A8), while SSD397 had mutations only in the promoter region of *TdHsp26-B1* (B4, B5, and B6).

Both *TdHsp26-A1* and *TdHsp26-B1* were significantly upregulated in SSD69 following heat stress, with expression levels ranging from a 10.62-fold increase at 4hPS to a 6.62-fold increase at 1hPR for *TdHsp26-A1*, and from a 9.32-fold increase at 4hPS to a 5.61-fold increase at 1hPR for *TdHsp26-B1*. In contrast, SSD397 showed a markedly lower level of gene expression for both genes, with *TdHsp26-A1* expression dropping from a 2.84-fold change at 4hPS to 1.2-fold at 1hPR, and *TdHsp26-B1* expression decreasing from 2.62-fold at 4hPS to −0.28-fold at 1hPR.

Both lines demonstrated higher expression of the *TdHsp26-A1* gene compared to the *TdHsp26-B1* gene, consistent with previous findings (Comastri et al., 2018).

3.5. Heat stress response in tillering stage

Based on the results obtained at seedlings stage and the position of SNPs in the gene of interest 7 genotypes (5 SSDs and 2 varieties) were chosen for the stress test at this stage: based on SNPs position in *TdHsp26*, five haplotypes: and two cultivars, Svevo and Kronos, were chosen as reference in the heat stress response.

Phenotyping analysis was performed after morphological, physiological and stress indices assessment.

3.5.1. Morphological traits

Leaf area was measured at 48 hours post-stress (48hPS) and one-week post-stress (1WPS) because no significant morphological differences were detectable at 4 hours post-stress (4hPS) (Suppl. Fig. 3b). The number of culms (Suppl. Fig. 3e) and plant height (Suppl. Fig. 3f) were assessed at 1WPS. Significant differences in leaf area were observed between stressed and control plants at 1WPS for SSD415 and between C48h, S48h and C1W, S1W for Kronos, with stressed plants showing a reduction in leaf area compared to controls (Suppl. Fig. 3b).

Stressed SSD244 and SSD397 exhibited a significant reduction in plant height at S1W ($P < 0.05$ and $P < 0.01$, respectively) (Suppl. Fig. 3f). Kronos showed a decreased number of culms at S1W, while no significant changes in the number of culms were observed in other genotypes between stressed and control plants (Suppl. Fig. 3e).

3.5.2. Stomatal resistance

Stomatal resistance (r_s, sec x cm^{-1}) is a key physiological trait used to estimate gas exchange, including CO_2 absorption through the leaves and water loss through transpiration, by assessing the opening and closing of stomata.

Under heat stress, all tested genotypes exhibited reduced stomatal resistance at 4 hours post-stress (4hPS), indicating increased stomatal conductance (Fig. 5) (Suppl. Fig. 4a). At 48 hours post-stress (48hPS), stomatal resistance in all genotypes returned to levels comparable to control plants, except for SSD397, which continued to show reduced stomatal resistance (Fig. 5) (Suppl. Fig. 4b). By one week post-stress (S1W), SSD397 and Svevo showed lower stomatal resistance under stress compared to control plants (Fig. 5) (Suppl. Fig. 4c).

3.5.3. Leaf temperature

Leaf temperature, measured as infrared leaf temperature, was used as an effective indicator of heat stress tolerance. After 4 hours at 38°C, all tested genotypes exhibited an increase in canopy temperature. Notably, SSD397 showed a greater increase in temperature compared to all other genotypes ($p<0.05$), indicating higher susceptibility to heat stress (Fig. 6a).

Additional physiological traits were analyzed to assess heat stress tolerance. Relative Water Content (RWC) was not a reliable indicator of tolerance, as leaf hydration levels decreased during heat stress (4hPS) but returned to normal in all tested genotypes by 1WPS (Suppl. Fig. 3c).

Canopy Temperature Depression (CTD), which estimates overall plant water status and its correlation with heat stress, was also measured (Kumar et al., 2017). After heat stress (4hPS), SSD69 and Svevo exhibited significantly higher CTD values (6.31°C and 6.35°C, respectively), indicating better water status, while SSD397 had the lowest CTD value (4.87°C) (Suppl. Fig. 3d). At S1W, CTD values were recorded as baseline (T0).

3.5.4. Genotypes ranking with ASR (Average Sum Ranks) and yield

Using iPASTIC, the Average Sum Ranks (ASR) based on nine different indices was calculated: Tolerance, Mean Productivity, Geometric Mean Productivity, Harmonic Mean, Stress Susceptibility Index, Stress Tolerance Index, Yield Index, Yield Stability Index, and Relative Stress Index. A lower ASR value indicates higher tolerance. The ASR was determined by measuring the number of seeds per plant for various genotypes under both control and stress conditions.

The analysis revealed that SSD69, SSD178, and Svevo had the lowest ASR values, indicating higher tolerance to heat stress. In contrast, SSD397 and SSD244 had the highest ASR values, indicating lower tolerance. SSD415 and Kronos fell in between (Fig. 6b).

Additionally, the number of seeds per spike was assessed as a key trait for evaluating yield. SSD397 and Kronos experienced the greatest reduction in seed production due to heat stress, with decreases of 63.9 % and 36.3 %, respectively. Conversely, SSD69, SSD178, SSD244, SSD415, and Svevo did not show significant changes in seed production under heat stress.

3.5.5. Oxidative stress and ROS accumulation

Heat stress leads to an overproduction of antioxidant enzymes, which help mitigate the accumulation of reactive oxygen species (ROS) in plant cells (Medina et al., 2021).

Among the genotypes tested, SSD178, SSD244, SSD397, SSD415, and Kronos exhibited an increase in H_2O_2 content between 4 hours post-stress (4hPS) and 1 hour post-recovery (1hPR). In contrast, SSD69 and Svevo did not show a significant increase in H_2O_2 immediately after the stress. After one week of stress, increases in H_2O_2 content were observed as follows: 22.31 % in SSD69, 26.87 % in SSD178, 54.75 % in SSD397, and 16.7 % in Kronos, indicating a delayed accumulation of H_2O_2 in these potentially tolerant lines (Fig. 7; Suppl. Fig. 5a).

Regarding malondialdehyde (MDA) content, SSD69, SSD244, and Svevo did not show an increase. SSD397 experienced a significant increase of about 100 % after 4hPS and 62.48 % after one week of stress. SSD415 also showed an increase of 23.56 % after 4hPS and 67.43 % after one week of stress. SSD178 exhibited a 55.12 % increase in MDA content after 1hPR compared to the control, while Kronos showed a late increase of 36.33 % after one week of stress.

3.5.6. TdHsp26 Gene Expression at tillering stage

Unlike at the seedling stage, *TdHsp26-B1* exhibited reduced expression at tillering in both SSD69 and SSD397, even before stress application (T0, control sample). After heat stress, *TdHsp26-A1* and *TdHsp26-B1* genes were significantly upregulated in SSD69, with expression levels increasing from 1.66-fold at 4hPR to 1.30-fold at 1hPR for *TdHsp26-A1*, and from 1.75-fold at 4hPR to 1.03-fold at 1hPR for *TdHsp26-B1* (Fig. 4b). SSD397 showed an increase in expression for both genes: *TdHsp26-A1* increased from 1.38-fold to 1.19-fold and *TdHsp26-B1* from 1.53-fold to 1.40-fold from 4hPS to 1hPR (Fig. 4b). These results represent a semi-quantitative analysis based on TAE 1x agarose gel, comparing the target gene band to the housekeeping gene band. Notably, *TdHsp26-B1* in SSD397 did not show a significant reduction

between 4hPS and 1hPR.

A principal component analysis (PCA) was conducted to identify the most influential agro-morphological traits related to heat resistance, considering all variables and stages (Graphical Abstract, Fig. 8). The first two principal components accounted for 57.7 % of the total variation. At 4hPS, controls and stressed SSDs clustered into two distinct groups, indicating the effect of the heat treatment. However, at one-week post-stress, clustering patterns changed. Control and stressed samples of SSD69 and SSD178 were closely grouped, suggesting potential heat tolerance for these genotypes. In contrast, control and stressed samples of SSD397 were separated, indicating greater susceptibility. Additionally, Relative Water Content (RWC), Stomatal Resistance (SR), and Canopy Temperature Depression (CTD) were highly correlated at 4hPS, while morphological traits such as plant canopy and leaf area showed strong correlations (Fig. 8a).

At S1W, PCA results revealed that morphological traits (number of culms, leaf area, plant height, and number of leaves) clustered separately from physiological traits (SR, infrared temperature), highlighting the utility of this phenotyping method for assessing wheat stress resistance (Fig. 8b). In both PCA plots, infrared temperature and CTD were inversely correlated, as expected (Fig. 8).

4. Discussion and conclusions: from genotypes to gene - ecology

Over the last decade, various omics methodologies have significantly transformed how biotechnologists and plant breeders explore the fundamental mechanisms of stress tolerance and cellular homeostasis (Yadav et al., 2022). The increase in average winter temperatures has severely impacted wheat productivity and planting areas (Farhad et al., 2023).

To prepare for adaptation to climate change, it is essential to segregate the effects of a specific aspect for influences on yield because fluctuations in diverse factors typically need different adaptation approaches.

To adapt to climate change, it is crucial to separate the effects of specific factors on yield, as fluctuations in different variables often require distinct adaptation strategies. The exploration of germplasm and the exploitation of novel alleles from the wild gene pool are becoming increasingly important due to the growing demands for global food supply, driven by human population growth and by climate changes (Farhad et al., 2023; Pignone et al., 2015).

The domestication and cultivation of tetraploid wheat in the Mediterranean Basin were strongly influenced by environmental conditions and by farmers' selection strategies for desirable agronomic and end-use traits. This likely contributed to the development of many well-adapted durum wheat landraces within their agro-ecological zones of origin (Lopes et al., 2015).

Modern breeding employs the strategy of "allele shuffling" (Adel and Carels, 2023), similar to shuffling SNPs through crossing and screening of subsequent recombinant lines. However, phenotyping is necessary to link SNPs to specific traits before assigning roles to these SNPs and identifying any efficient SNP combinations. By phenotypically characterizing haplotypes under heat stress conditions, it is possible to evaluate which haplotypes are candidates for selection and testing in specific environments and which haplotypes are no longer of interest (Bevan et al., 2017).

This study focuses on 17 haplotypes within the set of germplasm genotypes tested. Among these, haplotypes HA1, HA2, and HA3 are the most prevalent, each representing multiple SSD genotypes. Of the 17 haplotypes, 13 are associated with single SSD genotypes. Seven originate from the Hellenic Peninsula (HA10, HA11, HA12, HA13, HA14, HA15, and HA17), four from the Fertile Crescent area (HA3, HA6, HA12, and HA16, Fig. 2), one from North Africa (HA4, SSD69), and one from Ethiopia (HA9, SSD244), reflecting the origin and migration patterns of wheat.

Two haplotypes, HA4 and HA13, corresponding to SSD69 and SSD397, carry unique SNPs located in the promoter region and identified as B19 and B5, respectively (Suppl. Table 5).

SSD69, classified as a heat-tolerant genotype, originated in Morocco and was selected for its ability to thrive in arid and hot environments. SSD397, originating from Crete, is more influenced by the Mediterranean temperate climate, supporting the previously described maritime migration route from Greece and Crete to Libya, and then from the Sicilian peninsula to the coasts of Tunisia, Algeria, and Morocco (Feldman, 2001).

These findings reinforce Greece's role as a transit route for cereals entering Europe and suggest that Greece may have been one of the first European sites where the cultivation of this type of grain was adopted (Janni et al., 2019).

Special attention should be given to the HA5 haplotype and, more broadly, to genotypes originating from the U.S. The introduction of durum wheat to North, Central, and South America began with the Spanish and Portuguese in South America, followed by Europeans in the United States, Canada, and Australia. Additionally, global breeding programs from the International Maize and Wheat Improvement Center (CIMMYT) and the International Center for Agricultural Research in the Dry Areas (ICARDA) have played a significant role (Balfourier et al., 2019). This history helps explain the similarities in SNPs found among genotypes within the HA3 haplotype.

The distribution of *TdHsp26* haplotypes across different countries supports the idea of durum wheat diversification starting from its center of origin in the Fertile Crescent and spreading to North Africa and Ethiopia (Janni et al., 2018; Kidane et al., 2017; Royo et al., 2020).

The "Italian" genotypes can be grouped with North African genotypes (from Algeria and Ethiopia), suggesting that wheat was likely brought to Southern Italy from North Africa (Janni et al., 2018; Moragues et al., 2006; Oliveira et al., 2012). These findings point to the strong influence of the ancient Roman Empire's expansion, which promoted trade relationships between North Africa and Europe. By the beginning of the first millennium, North Africa had become the principal source of much of the wheat consumed during that period (Garnsey et al., 1983). According to Scarascia Mugnozza (1989), one consequence of Italian colonialism in Ethiopia during the first half of the 20th century was the importation and use of Italian durum wheat germplasm (Janni et al., 2019).

At high temperatures and under low humidity conditions, SSD69 exhibited a reduced canopy temperature and increased canopy temperature depression (CTD) values, along with improved transpiration due to greater stomatal conductance. This supports the idea that genotypes with higher CTD values and cooler canopy temperatures under heat stress utilize available soil moisture more effectively to cool the canopy through transpiration (Reynolds et al., 2020). The delayed senescence observed in SSD69 further supports its ability to withstand heat stress and enhance yield. In contrast, SSD397 displayed higher canopy temperatures and lower CTD values, indicating its inability to activate an efficient transpiration process and mitigate the effects of heat stress.

From a methodological perspective, this work exemplifies Eco-TILLING (Bajaj et al., 2016) and underscores the importance of combining genetic resources, innovative genomic technologies, and deep phenotyping to improve durum wheat's response to heat stress. It also highlights that genetic resources with an evolutionary history shaped by environmental conditions and dietary practices can serve as reservoirs of new traits valuable for countering the effects of climate change. Selecting related traits within target crops may be crucial in developing novel genetic variants that were lost during durum wheat domestication and cultivation, but for which modern consumers are showing increasing interest (Graziano et al., 2022; Shafeeq-ur-Rahman et al., 2020).

This study supports the notion that exploiting ex situ genetic resources is essential for enhancing plant adaptation to a changing environment, emphasizing the importance of haplotype-based breeding in

designing heat-adaptive durum wheat genotypes (Mehvish et al., 2023; Rai and Tyagi, 2022; Singh et al., 2024). The targeted analysis of the small Hsp26 gene in durum wheat germplasm led to the identification of SNPs correlated with increased adaptability to heat stress. The germplasm collection can be further analyzed to identify target genes and combine beneficial alleles in more adaptable genotypes.

Identifying genotypes with improved heat tolerant and testing them for other adaptive traits can further enhance the genetic diversity available for durum wheat breeding. There is a pressing need to develop manageable collections and new molecular methods for the identification of stress-tolerant genotypes.

This work highlights the effectiveness of the SSD approach in detecting and utilizing the extensive genetic variability present in germplasm resources. SSD has proven to be a valuable tool for developing core collections in crops like wheat, chickpea, barley, and lentils (Guerra-García et al., 2021; Kigoni et al., 2023; Rocchetti et al., 2022).

Furthermore, increasing genetic diversity through SSD lines is crucial for identifying marker-trait associations and predicting phenotypes based on genotypic data. Advances in SSD methodology, such as combining speed breeding techniques with SSD, have been proposed in rice.

Despite significant progress in genomic analysis, phenotyping remains a bottleneck, although it is essential for accurately characterizing the potential of novel breeding traits. This study advances phenotyping knowledge related to heat resilience by identifying key traits to consider when characterizing durum wheat germplasm.

Integrating genetic knowledge with phenotypic, ecological, and historical considerations, often referred to as gene-ecology, paves the way for a sustainable and holistic approach to breeding for resilience to climate change.

CRediT authorship contribution statement

Nelson Marmiroli: Writing – original draft, Funding acquisition, Conceptualization. **Michela Janni:** Writing – original draft, Supervision, Conceptualization. **Elena Dembech:** Visualization, Investigation, Formal analysis. **Giorgio Impollonia:** Data curation. **Domenico Pignone:** Writing – review & editing, Conceptualization. **Valentina Buffagni:** Methodology. **Filippo Vurro:** Data curation. **Nadia Palermo:** Methodology, Investigation, Data curation.

Declaration of Competing Interest

The authors declare that they have no known competing financial interests or personal relationships that could have appeared to influence the work reported in this paper.

Data Availability

Data are available upon request. Benefits Generated: A research collaboration was developed with scientists of different institutions and all collaborators are included as co-authors, the results of research have been shared with a broader scientific community.

Acknowledgments

The authors wish to thank the CINSA Consortium for financial support for the preparation of this review. The authors wish to acknowledge the support of the project SIMBA funded by the European Union's Horizon 2020 research and innovation program under grant agreement No. 818431, CONNECTFARMS SusCrop- ERA-NET funded under the Joint Call of the Cofund ERA-Nets SusCrop (Grant N° 573 771134).

Author Contribution

MN, JM conceived the study; BV contributed to pre-processing and getting the genotype data; PN performed the experiments, analysed the data and conceived the images; JM and NM led the writing of the manuscript, VF performed the PCA analysis, IG provide the algorithm to analyse the thermal data, PD provide the SSD lines and help in conceiving the discussion, NHT review of the manuscript, ED performed the protein analysis. All authors contributed critically to the drafts and gave final approval for publication.

Author Agreement Statement

We the undersigned declare that this manuscript is original, has not been published before and is not currently being considered for publication elsewhere. We confirm that the manuscript has been read and approved by all named authors and that there are no other persons who satisfied the criteria for authorship but are not listed. We further confirm that the order of authors listed in the manuscript has been approved by all of us. Due to the inclusion of additional data regarding the protein structure, we all agree to include Elena Dembech as coauthor. We understand that the Corresponding Author is the sole contact for the Editorial process. She is responsible for communicating with the other authors about progress, submissions of revisions and final approval of proofs.

Appendix A. Supporting information

Supplementary data associated with this article can be found in the online version at doi:10.1016/j.envexpbot.2024.105986.

References

Adel, S., Carels, N., 2023. Plant Tolerance to Drought Stress with Emphasis on Wheat. Plants 12, 2170. https://doi.org/10.3390/plants12112170.

Akter, N., Rafiqul Islam, M., 2017. Heat stress effects and management in wheat. A review. Agron. Sustain. Dev. 37, 37. https://doi.org/10.1007/s13593-017-0443-9.

Anand, A., Subramanian, M., Kar, D., 2023. Breeding techniques to dispense higher genetic gains. Front. Plant Sci. 13.

Backes, G., 2013. TILLING and EcoTILLING. In: Lübberstedt, T., Varshney, R.K. (Eds.), Diagnostics in Plant Breeding. Springer Netherlands, Dordrecht, pp. 145–165. https://doi.org/10.1007/978-94-007-5687-8_7.

Bajaj, D., Srivastava, R., Nath, M., Tripathi, S., Bharadwaj, C., Upadhyaya, H.D., Tyagi, A. K., Parida, S.K., 2016. EcoTILLING-Based Association Mapping Efficiently Delineates Functionally Relevant Natural Allelic Variants of Candidate Genes Governing Agronomic Traits in Chickpea. Front. Plant Sci. 7. https://doi.org/10.3389/fpls.2016.00450.

Balfourier, F., Bouchet, S., Robert, S., De Oliveira, R., Rimbert, H., Kitt, J., Choulet, F., Paux, E., 2019. Worldwide phylogeography and history of wheat genetic diversity. Sci. Adv. 5, eaav0536. https://doi.org/10.1126/sciadv.aav0536.

Barlow, K.M., Christy, B.P., O'Leary, G.J., Riffkin, P.A., Nuttall, J.G., 2015. Simulating the impact of extreme heat and frost events on wheat crop production: A review. Field Crops Res. 171, 109–119. https://doi.org/10.1016/j.fcr.2014.11.010.

Basha, E., Friedrich, K.L., Vierling, E., 2006. The N-terminal arm of small heat shock proteins is important for both chaperone activity and substrate specificity. J. Biol. Chem. 281, 39943–39952. https://doi.org/10.1074/jbc.M607677200.

Bassi, F.M., Bentley, A.R., Charmet, G., Ortiz, R., Crossa, J., 2016. Breeding schemes for the implementation of genomic selection in wheat (Triticum spp. Plant Sci. 242, 23–36. https://doi.org/10.1016/j.plantsci.2015.08.021.

Bevan, M.W., Uauy, C., Wulff, B.B.H., Zhou, J., Krasileva, K., Clark, M.D., 2017. Genomic innovation for crop improvement. Nature 543, 346–354. https://doi.org/10.1038/nature22011.

Bondino, H.G., Valle, E.M., ten Have, A., 2012. Evolution and functional diversification of the small heat shock protein/α-crystallin family in higher plants. Planta 235, 1299–1313. https://doi.org/10.1007/s00425-011-1575-9.

Borrill, P., Harrington, S.A., Uauy, C., 2019. Applying the latest advances in genomics and phenomics for trait discovery in polyploid wheat. Plant J. 97, 56–72. https://doi.org/10.1111/tpj.14150.

Buffagni, V., 2019. Studying durum wheat genetic diversity: a molecular approach to identify new alleles for drought resilience (Doctoral thesis). Univ. à degli Stud. di Parma. Dipartimento di Sci. Chim., della vita e della sostenibilità Ambient.

Ceglar, A., Toreti, A., Zampieri, M., Royo, C., 2021. Global loss of climatically suitable areas for durum wheat growth in the future. Environ. Res. Lett. 16, 104049. https://doi.org/10.1088/1748-9326/ac2d68.

Chandrasekhar, K., Nashef, K., Ben-David, R., 2017. Agronomic and genetic characterization of wild emmer wheat (Triticum turgidum subsp. dicoccoides) introgression lines in a bread wheat genetic background. Genet Resour. Crop Evol. 64, 1917–1926. https://doi.org/10.1007/s10722-016-0481-1.

Comastri, A., Janni, M., Simmonds, J., Uauy, C., Pignone, D., Nguyen, H.T., Marmiroli, N., 2018. Heat in wheat: exploit reverse genetic techniques to discover

new alleles within the Triticum durum sHsp26 family. Front. Plant Sci. 9. https://doi.org/10.3389/fpls.2018.01337.
Danzi, D., Briglia, N., Petrozza, A., Summerer, S., Povero, G., Stivaletta, A., Cellini, F., Pignone, D., De Paola, D., Janni, M., 2019. Can High Throughput Phenotyping Help Food Security in the Mediterranean Area? Front. Plant Sci. 10, 15. https://doi.org/10.3389/fpls.2019.00015.
Danzi, D., De Paola, D., Petrozza, A., Summerer, S., Cellini, F., Pignone, D., Janni, M., 2022. The use of near-infrared imaging (NIR) as a fast non-destructive screening tool to identify drought-tolerant wheat genotypes. Agriculture 12, 537. https://doi.org/10.3390/agriculture12040537.
Dong, Y., Xu, L., Wang, Q., Fan, Z., Kong, J., Bai, X., 2014. Effects of exogenous nitric oxide on photosynthesis, antioxidative ability, and mineral element contents of perennial ryegrass under copper stress. J. Plant Interact. 9, 402–411. https://doi.org/10.1080/17429145.2013.845917.
Ezcurra, I., Wycliffe, P., Nehlin, L., Ellerström, M., Rask, L., 2000. Transactivation of the Brassica napus napin promoter by ABI3 requires interaction of the conserved B2 and B3 domains of ABI3 with different cis-elements: B2 mediates activation through an ABRE, whereas B3 interacts with an RY/G-box. The Plant journal: for cell and molecular biology 24. https://doi.org/10.1046/j.1365-313x.2000.00857.x.
Farhad, M., Kumar, U., Tomar, V., Bhati, P.K., Krishnan, J., Kishowar-E-Mustarin, N., Barek, V., Brestic, M., Hossain, A., 2023. Heat stress in wheat: a global challenge to feed billions in the current era of the changing climate. Front. Sustain. Food Syst. 7. https://doi.org/10.3389/fsufs.2023.1203721.
Feldman, 2001. URL https://www.scirp.org/(S(vtj3fa45qm1ean45vvffcz55))/reference/ReferencesPapers.aspx?ReferenceID=408546 (accessed 11.22.23).
Fontana, G., Toreti, A., Ceglar, A., De Sanctis, G., 2015. Early heat waves over Italy and their impacts on durum wheat yields. Nat. Hazards Earth Syst. Sci. 15, 1631–1637. https://doi.org/10.5194/nhess-15-1631-2015.
Galluzzi, G., Seyoum, A., Halewood, M., López Noriega, I., Welch, E.W., 2020. The role of genetic resources in breeding for climate change: the case of public breeding programmes in eighteen developing countries. Plants 9, 1129. https://doi.org/10.3390/plants9091129.
Garnsey, P., Hopkins, K., Whittaker, C.R., 1983. Trade in the ancient economy. Chatto & Windus.
Giovenali, G., Kuzmanović, L., Capoccioni, A., Ceoloni, C., 2023. The response of chromosomally engineered durum wheat-thinopyrum ponticum recombinant lines to the application of heat and water-deficit stresses: effects on physiological, biochemical and yield-related traits. Plants 12, 704. https://doi.org/10.3390/plants12040704.
Graziano, S., Agrimonti, C., Marmiroli, N., Gullì, M., 2022. Utilisation and limitations of pseudocereals (quinoa, amaranth, and buckwheat) in food production: a review. Trends Food Sci. Technol. 125, 154–165. https://doi.org/10.1016/j.tifs.2022.04.007.
Guerra-García, A., Gioia, T., von Wettberg, E., Logozzo, G., Papa, R., Bitocchi, E., Bett, K. E., 2021. Intelligent characterization of lentil genetic resources: evolutionary history, genetic diversity of germplasm, and the need for well-represented collections. Curr. Protoc. 1, e134. https://doi.org/10.1002/cpz1.134.
Guzman, 2016. URL https://www.academia.edu/32972169/Guzman_C_2016_Wheat_quality_improvement_at_CIMMYT_and_genomic_selection_A_and_TG_pdf (accessed 11.21.23).
Hasan, N., Choudhary, S., Naaz, N., Sharma, N., Laskar, R.A., 2021. Recent advancements in molecular marker-assisted selection and applications in plant breeding programmes. J. Genet. Eng. Biotechnol. 19, 128. https://doi.org/10.1186/s43141-021-00231-1.
Hieno, A., Naznin, H.A., Inaba-Hasegawa, K., Yokogawa, Tomoko, Hayami, N., Nomoto, M., Tada, Y., Yokogawa, Takashi, Higuchi-Takeuchi, M., Hanada, K., Matsui, M., Ikeda, Y., Hojo, Y., Hirayama, T., Kusunoki, K., Koyama, H., Mitsuda, N., Yamamoto, Y.Y., 2019. Transcriptome analysis and identification of a transcriptional regulatory network in the response to H_2O_2. Plant Physiol. 180, 1629–1646. https://doi.org/10.1104/pp.18.01426.
Janni, M., Cadonici, S., Bonas, U., Grasso, A., Dahab, A.A.D., Visioli, G., Pignone, D., Ceriotti, A., Marmiroli, N., 2018. Gene-ecology of durum wheat HMW glutenin reflects their diffusion from the center of origin. Sci. Rep. 8, 16929. https://doi.org/10.1038/s41598-018-35251-4.
Janni, M., Coppede, N., Bettelli, M., Briglia, N., Petrozza, A., Summerer, S., Vurro, F., Danzi, D., Cellini, F., Marmiroli, N., Pignone, D., Iannotta, S., Zappettini, A., 2019. In vivo phenotyping for the early detection of drought stress in tomato. Plant Phenomics 2019, 1–10. https://doi.org/10.34133/2019/6168209.
Janni, M., Gullì, M., Maestri, E., Marmiroli, M., Valliyodan, B., Nguyen, H.T., Marmiroli, N., 2020. Molecular and genetic bases of heat stress responses in crop plants and breeding for increased resilience and productivity. J. Exp. Bot. 71, 3780–3802. https://doi.org/10.1093/jxb/eraa034.
Jenkins, D., Juba, N., Crawford, B., Worthington, M., Hummel, A., 2023. Regulation of plants developed through new breeding techniques must ensure societal benefits. Nat. Plants 9, 679–684. https://doi.org/10.1038/s41477-023-01403-2.
Kidane, Y.G., Hailemariam, B.N., Mengistu, D.K., Fadda, C., Pè, M.E., Dell'Acqua, M., 2017. Genome-wide association study of septoria tritici blotch resistance in ethiopian durum wheat landraces. Front. Plant Sci. 8, 1586. https://doi.org/10.3389/fpls.2017.01586.
Kigoni, M., Choi, M., Arbelaez, J.D., 2023. Single-Seed-SpeedBulks:' a protocol that combines 'speed breeding' with a cost-efficient modified single-seed descent method for rapid-generation-advancement in oat (Avena sativa L.). Plant Methods 19. https://doi.org/10.1186/s13007-023-01067-1.
Lescot, M., 2002. PlantCARE, a database of plant cis-acting regulatory elements and a portal to tools for in silico analysis of promoter sequences. Nucleic Acids Res. 30, 325–327. https://doi.org/10.1093/nar/30.1.325.
Liu, S., Liu, J., Zhang, Y., Jiang, Y., Hu, S., Shi, A., Cong, Q., Guan, S., Qu, J., Dan, Y., 2022. Cloning of the soybean *sHSP26* gene and analysis of its drought resistance. PHYTON 91, 1465–1482. https://doi.org/10.32604/phyton.2022.018836.
Lopes, M.S., El-Basyoni, I., Baenziger, P.S., Singh, S., Royo, C., Ozbek, K., Aktas, H., Ozer, E., Ozdemir, F., Manickavelu, A., Ban, T., Vikram, P., 2015. Exploiting genetic diversity from landraces in wheat breeding for adaptation to climate change. EXBOTJ 66, 3477–3486. https://doi.org/10.1093/jxb/erv122.
Lu, L., Liu, H., Wu, Y., Yan, G., 2022. Wheat genotypes tolerant to heat at seedling stage tend to be also tolerant at adult stage: The possibility of early selection for heat tolerance breeding. Crop J. 10, 1006–1013. https://doi.org/10.1016/j.cj.2022.01.005.
Maestri, E., Klueva, N., Perrotta, C., Gulli, M., Nguyen, H.T., Marmiroli, N., 2002. Molecular genetics of heat tolerance and heat shock proteins in cereals. Plant Mol. Biol. 48, 667–681. https://doi.org/10.1023/A:1014826730024.
Mazzucotelli, E., Sciara, G., Mastrangelo, A.M., Desiderio, F., Xu, S.S., Faris, J., Hayden, M.J., Tricker, P.J., Ozkan, H., Echenique, V., Steffenson, B.J., Knox, R., Niane, A.A., Udupa, S.M., Longin, F.C.H., Marone, D., Petruzzino, G., Corneti, S., Ormanbekova, D., Pozniak, C., Roncallo, P.F., Mather, D., Able, J.A., Amri, A., Braun, H., Ammar, K., Baum, M., Cattivelli, L., Maccaferri, M., Tuberosa, R., Bassi, F. M., 2020. The Global Durum Wheat Panel (GDP): An International Platform to Identify and Exchange Beneficial Alleles. Front. Plant Sci. 11, 569905. https://doi.org/10.3389/fpls.2020.569905.
Medina, E., Kim, S.-H., Yun, M., Choi, W.-G., 2021. Recapitulation of the Function and Role of ROS Generated in Response to Heat Stress in Plants. Plants 10, 371. https://doi.org/10.3390/plants10020371.
Mehvish, A., Aziz, A., Bukhari, B., Qayyum, H., Mahmood, Z., Baber, M., Sajjad, M., Pang, X., Wang, F., 2023. Identification of Single-Nucleotide Polymorphisms (SNPs) Associated with Heat Tolerance at the Reproductive Stage in Synthetic Hexaploid Wheats Using GWAS. Plants 12, 1610. https://doi.org/10.3390/plants12081610.
Mohi-Ud-Din, M., Siddiqui, N., Rohman, M., Jagadish, S.V.K., Ahmed, J.U., Hassan, M. M., Hossain, A., Islam, T., 2021. Physiological and biochemical dissection reveals a trade-off between antioxidant capacity and heat tolerance in bread wheat (Triticum aestivum L.). Antioxidants 10, 351. https://doi.org/10.3390/antiox10030351.
Moragues, M., Moral, L.F.G.D., Moralejo, M., Royo, C., 2006. Yield formation strategies of durum wheat landraces with distinct pattern of dispersal within the Mediterranean basin I: yield components. Field Crops Res. 95, 194–205. https://doi.org/10.1016/j.fcr.2005.02.009.
Ng, P.C., Henikoff, S., 2003. SIFT: predicting amino acid changes that affect protein function. Nucleic Acids Res. 31, 3812. https://doi.org/10.1093/nar/gkg509.
Nuttall, J.G., O'Leary, G.J., Panozzo, J.F., Walker, C.K., Barlow, K.M., Fitzgerald, G.J., 2015. Models of grain quality in wheat—a review. Field Crops Res. 202, 136–145. https://doi.org/10.1016/j.fcr.2015.12.011.
Oliveira, H.R., Campana, M.G., Jones, H., Hunt, H.V., Leigh, F., Redhouse, D.I., Lister, D. L., Jones, M.K., 2012. Tetraploid wheat landraces in the mediterranean basin: taxonomy, evolution and genetic diversity. PLoS One 7, e37063. https://doi.org/10.1371/journal.pone.0037063.
Patrignani, A., Ochsner, T.E., 2015. Canopeo: a powerful new tool for measuring fractional green canopy cover. Agron. J. 107, 2312–2320. https://doi.org/10.2134/agronj15.0150.
Pignone, D., De Paola, D., Rapanà, N., Janni, M., 2015. Single seed descent: a tool to exploit durum wheat (Triticum durum Desf.) genetic resources. Genet Resour. Crop Evol. 62, 1029–1035. https://doi.org/10.1007/s10722-014-0206-2.
Pour-Aboughadareh, A., Yousefian, M., Moradkhani, H., Moghaddam Vahed, M., Poczai, P., Siddique, K.H.M., 2019. *i* PASTIC: An online toolkit to estimate plant abiotic stress indices: *i* PASTIC to estimate plant abiotic stress indices. Appl. Plant Sci. 7, e11278. https://doi.org/10.1002/aps3.11278.
Pradhan, S., Babar, M.A., Bai, G., Khan, J., Shahi, D., Avci, M., Guo, J., McBreen, J., Asseng, S., Gezan, S., Baik, B.-K., Blount, A., Harrison, S., Sapkota, S., St. Amand, P., Kunwar, S., 2020. Genetic dissection of heat-responsive physiological traits to improve adaptation and increase yield potential in soft winter wheat. BMC Genom. 21, 315. https://doi.org/10.1186/s12864-020-6717-7.
Rai, M., Tyagi, W., 2022. Haplotype breeding for unlocking and utilizing plant genomics data. Front. Genet. 13. https://doi.org/10.3389/fgene.2022.1006288.
Ramkumar, G., Madhav, M.S., Devi, S.J.S.R., Prasad, M.S., Babu, V.R., 2015. Nucleotide variation and identification of novel blast resistance alleles of Pib by allele mining strategy. Physiol. Mol. Biol. Plants 21, 301. https://doi.org/10.1007/s12298-015-0284-4.
Reynolds, M., Chapman, Crespo-Herrera, Molero, 2020. Breeder friendly phenotyping - ScienceDirect [WWW Document]. URL https://www.sciencedirect.com/science/article/pii/S0168945219315699?via%3Dihub (accessed 1.18.23).
Rocchetti, L., Gioia, T., Logozzo, G., Brezeanu, C., Pereira, L.G., la Rosa, L.D., Marzario, S., Pieri, A., Fernie, A.R., Alseekh, S., Susek, K., Cook, D.R., Varshney, R. K., Agrawal, S.K., Hamwieh, A., Bitocchi, E., Papa, R., 2022. Towards the development, maintenance and standardized phenotypic characterization of single-seed-descent genetic resources for chickpea. Curr. Protoc. 2, e371. https://doi.org/10.1002/cpz1.371.
Rogers, H.J., Bate, N., Combe, J., Sullivan, J., Sweetman, J., Swan, C., Lonsdale, D.M., Twell, D., 2001. Functional analysis of cis-regulatory elements within the promoter of the tobacco late pollen gene g10. Plant Mol. Biol. 45, 577–585. https://doi.org/10.1023/A:1010695226241.
Royo, C., Nazco, R., Villegas, D., 2014. The climate of the zone of origin of Mediterranean durum wheat (Triticum durum Desf.) landraces affects their agronomic performance. Genet Resour. Crop Evol. 61, 1345–1358. https://doi.org/10.1007/s10722-014-0116-3.
Royo, C., Dreisigacker, S., Ammar, K., Villegas, D., 2020. Agronomic performance of durum wheat landraces and modern cultivars and its association with genotypic

variation in vernalization response (Vrn-1) and photoperiod sensitivity (Ppd-1) genes. Eur. J. Agron. 120, 126129. https://doi.org/10.1016/j.eja.2020.126129.
Savicka, M., Škute, N., 2010. (PDF) Eff ects of high temperature on malondialdehyde content, superoxide production and growth changes in wheat seedlings (Triticum aestivum L.). ResearchGate. https://doi.org/10.2478/v10055-010-0004-x.
Senthilkumar, M., Amaresan, N., Sankaranarayanan, A., 2021. Estimation of malondialdehyde (MDA) by thiobarbituric Acid (TBA) assay. Plant-Microbe Interact. 103–105. https://doi.org/10.1007/978-1-0716-1080-0_25.
Shafeeq-ur-Rahman, Xuebin, Q., Yatao, X., Ahmad, M.I., Shehzad, M., Zain, M., 2020. Silicon and its application methods improve physiological traits and antioxidants in triticum aestivum (L.) under cadmium stress. J. Soil Sci. Plant Nutr. 20, 1110–1121. https://doi.org/10.1007/s42729-020-00197-y.
Shirdelmoghanloo, H., Lohraseb, I., Rabie, H.S., Brien, C., Parent, B., Collins, N.C., 2016. Heat susceptibility of grain filling in wheat (Triticum aestivum L.) linked with rapid chlorophyll loss during a 3-day heat treatment. Acta Physiol. Plant 38, 208. https://doi.org/10.1007/s11738-016-2208-5.
Singh, P., Sundaram, K.T., Vinukonda, V.P., Venkateshwarlu, C., Paul, P.J., Pahi, B., Gurjar, A., Singh, U.M., Kalia, S., Kumar, A., Singh, V.K., Sinha, P., 2024. Superior haplotypes of key drought-responsive genes reveal opportunities for the development of climate-resilient rice varieties. Commun. Biol. 7, 1–11. https://doi.org/10.1038/s42003-024-05769-7.
Smart, R., Bingham, G.E., 1974. Rapid estimates of relative water content. Plant Physiol. 53, 258–260.
Tardieu, F., Tuberosa, R., 2010. Dissection and modelling of abiotic stress tolerance in plants. Curr. Opin. Plant Biol. 13, 206–212. https://doi.org/10.1016/j.pbi.2009.12.012.
Ullah, S., Bramley, H., Mahmood, T., Trethowan, R., 2020. The impact of emmer genetic diversity on grain protein content and test weight of hexaploid wheat under high temperature stress. J. Cereal Sci. 95, 103052. https://doi.org/10.1016/j.jcs.2020.103052.
Ullah, S., Bramley, H., Mahmood, T., Trethowan, R., 2021. Implications of emmer (Triticum dicoccon Schrank) introgression on bread wheat response to heat stress. Plant Sci. 304, 110738. https://doi.org/10.1016/j.plantsci.2020.110738.
Velikova, V., Fares, S., Loreto, F., 2008. Isoprene and nitric oxide reduce damages in leaves exposed to oxidative stress. Plant, Cell Environ. 31, 1882–1894. https://doi.org/10.1111/j.1365-3040.2008.01893.x.
Villain, P., Mache, R., Zhou, 1996. The mechanism of GT element-mediated cell type-specific transcriptional control. J. Biol. Chem. 271. https://doi.org/10.1074/jbc.271.51.32593.
Wang, L., Guo, Y., Jia, L., Chu, H., Zhou, S., Chen, K., Wu, D., Zhao, L., 2014. Hydrogen Peroxide Acts Upstream of Nitric Oxide in the Heat Shock Pathway in Arabidopsis Seedlings. Plant Physiol. 164, 2184–2196. https://doi.org/10.1104/pp.113.229369.
Xynias, I.N., Mylonas, I., Korpetis, E.G., Ninou, E., Tsaballa, A., Avdikos, I.D., Mavromatis, A.G., 2020. Durum wheat breeding in the mediterranean region: current status and future prospects. Agronomy 10, 432. https://doi.org/10.3390/agronomy10030432.
Yadav, M.R., Choudhary, M., Singh, J., Lal, M.K., Jha, P.K., Udawat, P., Gupta, N.K., Rajput, V.D., Garg, N.K., Maheshwari, C., Hasan, M., Gupta, S., Jatwa, T.K., Kumar, R., Yadav, A.K., Prasad, P.V.V., 2022. Impacts, tolerance, adaptation, and mitigation of heat stress on wheat under changing climates. Int. J. Mol. Sci. 23, 2838. https://doi.org/10.3390/ijms23052838.
Zampieri, M., Toreti, A., Ceglar, A., Naumann, G., Turco, M., Tebaldi, C., 2020. Climate resilience of the top ten wheat producers in the Mediterranean and the Middle East. Reg. Environ. Change 20, 41. https://doi.org/10.1007/s10113-020-01622-9.